
[All ETDs from UAB](#)

[UAB Theses & Dissertations](#)

1988

An Analytical Method To Optimize The Thermal Fatigue Life Of Multilayered Cylindrical Shells.

Gene Lamar Oliver
University of Alabama at Birmingham

Follow this and additional works at: <https://digitalcommons.library.uab.edu/etd-collection>

Recommended Citation

Oliver, Gene Lamar, "An Analytical Method To Optimize The Thermal Fatigue Life Of Multilayered Cylindrical Shells." (1988). *All ETDs from UAB*. 4374.
<https://digitalcommons.library.uab.edu/etd-collection/4374>

This content has been accepted for inclusion by an authorized administrator of the UAB Digital Commons, and is provided as a free open access item. All inquiries regarding this item or the UAB Digital Commons should be directed to the [UAB Libraries Office of Scholarly Communication](#).

INFORMATION TO USERS

The most advanced technology has been used to photograph and reproduce this manuscript from the microfilm master. UMI films the text directly from the original or copy submitted. Thus, some thesis and dissertation copies are in typewriter face, while others may be from any type of computer printer.

The quality of this reproduction is dependent upon the quality of the copy submitted. Broken or indistinct print, colored or poor quality illustrations and photographs, print bleedthrough, substandard margins, and improper alignment can adversely affect reproduction.

In the unlikely event that the author did not send UMI a complete manuscript and there are missing pages, these will be noted. Also, if unauthorized copyright material had to be removed, a note will indicate the deletion.

Oversize materials (e.g., maps, drawings, charts) are reproduced by sectioning the original, beginning at the upper left-hand corner and continuing from left to right in equal sections with small overlaps. Each original is also photographed in one exposure and is included in reduced form at the back of the book. These are also available as one exposure on a standard 35mm slide or as a 17" x 23" black and white photographic print for an additional charge.

Photographs included in the original manuscript have been reproduced xerographically in this copy. Higher quality 6" x 9" black and white photographic prints are available for any photographs or illustrations appearing in this copy for an additional charge. Contact UMI directly to order.

U·M·I

University Microfilms International
A Bell & Howell Information Company
300 North Zeeb Road, Ann Arbor, MI 48106-1346 USA
313/761-4700 800/521-0600



Order Number 8905889

**An analytical method to optimize the thermal fatigue life of
multilayered cylindrical shells**

Oliver, Gene Lamar, Ph.D.

The University of Alabama in Birmingham, 1988

Copyright ©1988 by Oliver, Gene Lamar. All rights reserved.

U·M·I

**300 N. Zeeb Rd.
Ann Arbor, MI 48106**



AN ANALYTICAL METHOD TO OPTIMIZE THE THERMAL FATIGUE LIFE OF
MULTILAYERED CYLINDRICAL SHELLS

by

GENE LAMAR OLIVER

A DISSERTATION

Submitted in partial fulfillment of the requirements for the
degree of Doctor of Philosophy in the Department
of Materials Engineering in the Graduate School,
The University of Alabama at Birmingham

BIRMINGHAM, ALABAMA

1988

Copyright by
Gene Lamar Oliver
1988

ABSTRACT OF DISSERTATION
GRADUATE SCHOOL, UNIVERSITY OF ALABAMA AT BIRMINGHAM

Degree Doctor of Philosophy Major Subject Materials Engineering

Name of Candidate Gene Lamar Oliver

Title AN ANALYTICAL METHOD TO OPTIMIZE THE THERMAL
FATIGUE LIFE OF MULTILAYERED CYLINDRICAL SHELLS

An analytical technique to determine and optimize the thermal fatigue life of multilayered cylindrical shells is presented. Finite difference heat flow and strain equations are developed and implemented, using Mendelson's and Manson's technique, into a thermo-elastic-plastic numerical model of a three layered cylindrical shell. The model calculates the temperature; the radial, tangential, and axial stresses; and the radial, tangential, and axial strains as a function of radius and time based on cylinder geometry, layer thicknesses, heat input, and thermomechanical and thermophysical properties of selected materials or alloys. Strain ranges are calculated for each of the layers of a design and are used to determine a tube's thermal fatigue life. Optimization is achieved by determining the fatigue life of different designs with varying layer thicknesses.

Details for the optimization of a steel-copper-steel composite cylindrical shell for one set of thermal and physical constraints is presented. The technique is

recommended as a design-analysis tool for cases involving axisymmetric thermal loading of cylindrical shells.

Abstract Approved by: Committee Chairman J. Barry Andrews
Program Director J. Barry Andrews
Date 9/2/88 Dean of Graduate School Anthony Band

ACKNOWLEDGMENTS

This research was conducted with the permission and assistance of American Cast Iron Pipe Company. The author wishes to thank the company as a whole, with special thanks to Paul W. Green, President; A. Tim Wuska, Technical Director; William E. Snow, (retired); and Ben C. Helton, Assistant Technical Director and Manager of Research, for their support and patience.

Thanks are also due to Dr. C. Hartley and my graduate committee, Drs. J.B. Andrews, R. Andrews, R. Thompson, and B. Patterson, all of the Materials Engineering Department, the University of Alabama at Birmingham, and especially to Professor A.E. Carden of the Engineering Mechanics Department of the University of Alabama for their advice, interest, and encouragement.

Finally, the author wishes to thank W.T. Adams, Jr., and Ms. D.A.W. Davis for their support and encouragement.

TABLE OF CONTENTS

	<u>Page</u>
ABSTRACT.....	iii
ACKNOWLEDGMENTS.....	v
LIST OF TABLES	vii
LIST OF FIGURES	viii
LIST OF SYMBOLS	xii
I. INTRODUCTION AND REVIEW OF LITERATURE.....	1
II. THEORY AND DERIVATION OF HEAT FLOW AND STRAIN EQUATIONS	7
Derivation of Finite Difference Heat Flow Equations ..	8
Derivation of Strain Equations for a Cylindrical Tube	20
III. IMPLEMENTATION OF HEAT FLOW AND STRAIN EQUATIONS INTO A THERMO-ELASTIC-PLASTIC NUMERICAL MODEL	41
IV. OPTIMIZATION OF A MULTILAYERED CYLINDRICAL SHELL WITH THE THERMO-ELASTIC-PLASTIC NUMERICAL MODEL	54
V. DISCUSSION OF RESULTS	97
VI. CONCLUSIONS AND RECOMENDATIONS.....	102
VII. LIST OF REFERENCES	105

LIST OF TABLES

<u>Table</u>		<u>Page</u>
1	Temperature Profile Calculations	42
2	Stress Analysis Logic Flow	52
3	Thermophysical Properties	56
4	Physical Dimensions, Mechanical Properties, and Thermal Loading Constraints	57
5	Results of Analysis of Composite Tube Designs	89

LIST OF FIGURES

<u>Figure</u>	<u>Page</u>
1	Total strain range versus cycles to failure for a typical steel..... 4
2	Drawing of a three layered cylindrical shell showing layer thicknesses, layer material, nodal system, and node types..... 9
3	Interface between ID surface and heat source..... 12
4	Nodal face of unit length in the z-direction..... 14
5	Plane view of copper-steel interface node..... 16
6	Section of a cylindrical tube showing cylindrical coordinate system..... 22
7	A single radial node of radius, "r," and thickness, "dr," showing the radial displacements, U, U+dU, and the resulting strains..... 23
8	Free body diagram showing forces acting on differential element of tube..... 25
9	Free body diagram of a half section of a tube showing forces acting in the y-direction. The inside radius is "a" and the outside radius is "b." The inside pressure is p_i and the outside pressure is p_o 27
10	Stress-strain curve of a typical steel showing the relationship between equivalent plastic and equivalent total strain..... 38
11	Equivalent total and equivalent plastic strain relationship for a typical steel obtained from stress-strain data at room temperature..... 39
12	A hysteresis loop showing loading and unloading paths of nodes that undergo elastic and elastic-plastic deformation..... 46

LIST OF FIGURES (Continued)

13	Hysteresis loop of an engineering alloy that has undergone compressive yielding followed by tensile yielding.....	48
14	Stress-strain curves at selected temperatures for 2 1/4% Cr-1% Mo steel.....	58
15	Stress-strain curves of OFHC copper at selected temperatures.....	59
16	Equivalent total and equivalent plastic strain relationship for 2 1/4% Cr-1% Mo steel at selected temperatures.....	60
17	Equivalent total and equivalent plastic strain relationship for OFHC copper at selected temperatures.....	61
18	Radial temperature profile in a composite tube with a 6 mm steel ID layer-18 mm copper middle layer-6 mm steel OD layer 1 second into the heating phase of a thermal cycle.....	62
19	Radial stress profile in a composite tube with a 6 mm steel ID layer-18 mm copper middle layer-6 mm steel OD layer 1 second into the heating phase of a thermal cycle.....	63
20	Tangential stress profile in a composite tube with a 6 mm steel ID layer-18 mm copper middle layer-6 mm steel OD layer 1 second into the heating phase of a thermal cycle.....	64
21	Axial stress profile in a composite tube with a 6 mm steel ID layer-18 mm copper middle layer-6 mm steel OD layer 1 second into the heating phase of a thermal cycle.....	65
22	Equivalent stress profile in a composite tube with a 6 mm steel ID layer-18 mm copper middle layer-6 mm steel OD layer 1 second into the heating phase of a thermal cycle.....	67
23	Equivalent plastic strain profile in a composite tube with a 6 mm steel ID layer-18 mm copper middle layer-6 mm steel OD layer 1 second into the heating phase of a thermal cycle.....	68

LIST OF FIGURES (Continued)

24	Radial temperature profile in a composite tube with a 6 mm steel ID layer-18 mm copper middle layer-6 mm steel OD layer 10 seconds into the heating phase of a thermal cycle.....	69
25	Radial stress profile in a composite tube with a 6 mm steel ID layer-18 mm copper middle layer-6 mm steel OD layer 10 seconds into the heating phase of a thermal cycle.....	70
26	Tangential stress profile in a composite tube with a 6 mm steel ID layer-18 mm copper middle layer-6 mm steel OD layer 10 seconds into the heating phase of a thermal cycle.....	71
27	Axial stress profile in a composite tube with a 6 mm steel ID layer-18 mm copper middle layer-6 mm steel OD layer 10 seconds into the heating phase of a thermal cycle.....	72
28	Equivalent stress profile in a composite tube with a 6 mm steel ID layer-18 mm copper middle layer-6 mm steel OD layer 10 seconds into the heating phase of a thermal cycle.....	73
29	Equivalent plastic strain profile in a composite tube with a 6 mm steel ID layer-18 mm copper middle layer-6 mm steel OD layer 10 seconds into the heating phase of a thermal cycle.....	74
30	Radial temperature profile in a composite tube with a 6 mm steel ID layer-18 mm copper middle layer-6 mm steel OD layer 35 seconds into a thermal cycle.....	76
31	Radial stress profile in a composite tube with a 6 mm steel ID layer-18 mm copper middle layer-6 mm steel OD layer 35 seconds into a thermal cycle.....	77
32	Tangential stress profile in a composite tube with a 6 mm steel ID layer-18 mm copper middle layer-6 mm steel OD layer 35 seconds into a thermal cycle.....	78
33	Axial stress profile in a composite tube with a 6 mm steel ID layer-18 mm copper middle layer-6 mm steel OD layer 35 seconds into a thermal cycle.....	79

LIST OF FIGURES (Continued)

34	Equivalent stress profile in a composite tube with a 6 mm steel ID layer-18 mm copper middle layer-6 mm steel OD layer 35 seconds into a thermal cycle.....	80
35	Equivalent plastic strain profile in a composite tube with a 6 mm steel ID layer-18 mm copper middle layer-6 mm steel OD layer 35 seconds into a thermal cycle.....	81
36	Transient temperature response of the ID node for 6 thermal cycles.....	82
37	Total radial and tangential strains as a function of thermal cycling.....	83
38	Principal total strains for one thermal cycle.....	84
39	Total strain differences (for the ID surface node) for a thermal cycle.....	86
40	Total strain range vs. cycles to failure for a 2 1/4% Cr-1% Mo steel at 427 C.....	87
41	Total strain range vs. cycles to failure for OFHC copper at 538 C.....	88
42	Thermal fatigue life of multilayered tube designs...	92
43	Thermal fatigue life of layers in multilayered tube designs with a 3 mm ID layer thickness.....	93
44	Thermal fatigue life of layers in multilayered tube designs with a 6 mm ID layer thickness.....	94
45	Thermal fatigue life of layers in multilayered tube designs with a 9 mm ID layer thickness.....	95
46	The radial displacement as calculated by the model, 10 seconds into a thermal cycle.....	98
47	Plot of total axial strain, ϵ_z , across the wall thickness of the tube demonstrating that a plane strain condition exists.....	99

LIST OF SYMBOLS

a	inside radius of tube
A_1, A_2	area of nodal faces
α_1, α_2	thermal diffusivity of composite node defined in text
α_{Cu}, α_{St}	thermal expansion coefficient of copper and steel
b	outside radius of tube
C_1, C_2	constants of integration
C_{pCu}, C_{pSt}	specific heat of copper and steel
du, dw	differential changes in lengths in the r and z directions
ϵ	strain
ϵ_{el}	elastic strain
ϵ_{ep}	equivalent plastic strain
ϵ_{et}	equivalent total strain
$\epsilon_r, \epsilon_\theta, \epsilon_z$	total strain in the $r, \theta,$ and z directions
$\epsilon_{rp}, \epsilon_{\theta p}, \epsilon_{zp}$	components of plastic strain in the $r, \theta,$ and z directions
$\Delta\epsilon_{rp}, \Delta\epsilon_{\theta p}, \Delta\epsilon_{zp}$	incremental components of plastic strain in the $r, \theta,$ and z directions for the current load increment

LIST OF SYMBOLS (Continued)

F_{Yi}	component of force in the y-direction from an internal pressure
F_{Yo}	component of force in the y-direction from an external pressure
G	one of Lamé's constants defined in the text
GA, GB, GC, GD, GE, GF	geometric correction factors
h_1, h_2	heat transfer coefficients for tube ID and OD
ID	inside diameter
k_{Cu}, k_{St}	thermal conductivity for copper and steel
λ	one of Lamé's constants defined in the text
N	number of cycles
N_f	cycles to failure
OD	outside diameter
P_i	internal pressure
P_o	external pressure
π	the constant pi
μ	Poisson's ratio
q_{in}	heat flow into a node
q_{out}	heat flow out of a node
q_{stored}	heat stored in a node
r	radius
r_i	inside radius
$r_{i,j}$	radial node, i is node position, j is time

LIST OF SYMBOLS (Continued)

r_o	outside radius
r, θ, z	directions in a cylindrical coordinate system
ρ_{Cu}, ρ_{St}	density of copper and steel
σ	normal stress
$\sigma_r, \sigma_\theta, \sigma_z$	normal stress in the $r, \theta,$ and z directions
$T_{i,j}$	temperature of the i th node at time j
TK1, TK2, TK3	layer thicknesses 1, 2, and 3, respectively
δt	time increment in heat flow equation

I. INTRODUCTION AND REVIEW OF LITERATURE

There are many applications in industry where transient thermal loading occurs on the inside diameter of cylindrical metal shells. These include heat exchanger tubing, piping in steam boilers, heavy duty truck brake drums, and permanent molds for casting metals, glasses, and ceramics. In all cases the tubular shapes are subject to a radial temperature gradient that induces thermal stresses. For small temperature gradients the stresses are elastic in nature, but if the temperature gradient is steep the thermal stresses exceed the yield strength of the material and plastic flow occurs. Repeated application of such thermal loads can lead to low cycle fatigue.

Elastic stress calculations for a long circular cylinder with a symmetrical temperature distribution about the axis were first performed by J.M.C. Duhamel¹ in 1838. Elastic solutions to several cases of thermal loading of cylindrical shapes have been presented by Timoshenko and Goodier.² The values of the displacement, U , stress, σ , and elastic strain, ϵ_{el} , from these solutions are valid as long as the stress does not exceed the yield strength of the material. In many cases the yield strength is exceeded, plastic flow occurs, and the values of stress calculated from elasticity theory are in error.

To better approximate the stresses and strains when yielding occurs, A. Mendelson and S.S. Manson³ developed a technique which accounts for plastic deformation due to thermal loading. Their technique consisted of deriving strain equations in terms of temperature and plastic yielding from the equilibrium, compatibility, and stress-strain relationships for the geometric shape and material under investigation. The strains were then calculated by an iterative technique taking into account the plastic flow of the material being analyzed. Stresses were then calculated from the general stress-strain equations.

Hanson⁴ used the Mendelson and Manson technique³ to compare the deformation and incremental theories of plasticity in the solution of two boundary value problems. The deformation theory assumed that the state of stress and strain existing in a body depended only on the current load. The deformation theory did not account for prior plastic strain due to prior loading and was therefore load path independent. Using the incremental theory, the loading and unloading cycle was divided into several small load increments. Stresses and strains were then calculated based on the small load increment, and any plastic strains that occurred during a load increment or prior load increments had an accumulative effect on the stress-strain state. The incremental theory's ability to account for plasticity due to small changes in load made stress and strain calculations load path dependent.

The first problem Hanson⁴ solved concerned the stress analysis of a solid cylindrical rod of 18-8 stainless steel quenched from 1000 F (538 C). A stress analysis was performed by both deformation and incremental theories of plasticity, and the results of each analysis were compared. The second problem was the stress analysis, by both deformation and incremental theories of plasticity, of a thin circular disc when heated on the outside diameter.

Hanson⁴ found that the results of the analysis from both deformation and incremental theories were in agreement until unloading occurred. Upon unloading, values of stress calculated from each theory deviated from each other. Hanson's experimental evidence indicated that the incremental theory was more predictive of the stress-strain state than was the deformation theory.

Manson⁵ used the Mendelson and Manson technique³ to determine the thermal fatigue life of a rotating solid disc when subjected to thermal loading. The load conditions were similar to those for discs in jet engines. Strain range values were calculated based on the mechanical and thermal loading cycles and a thermal fatigue life was predicted.

The objectives of this dissertation are to analyze and optimize a multilayer tube's thermal fatigue life when subjected to cyclic thermal loading on the inside surface. Figure 1 shows a log Total Strain Range ($\Delta\epsilon$) vs. log Cycles to Failure (N_f) diagram. This graph is often used to determine cyclic life at various strain ranges.⁶ It is evident from this graph that lower mechanical strain ranges

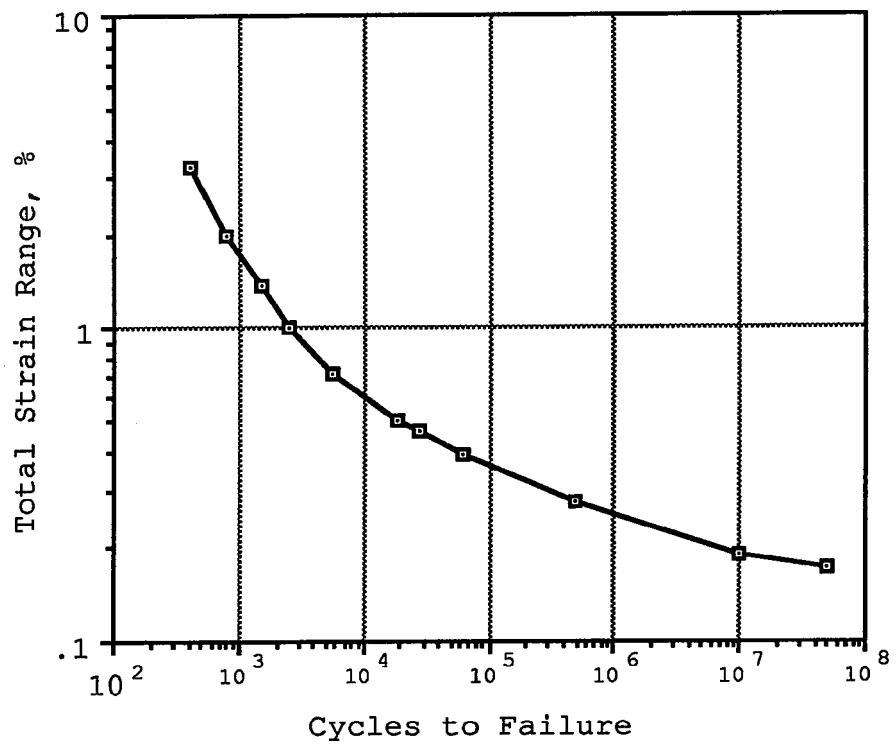


Figure 1. Total strain range versus cycles to failure for a typical steel.

result in high thermal fatigue lives. To improve the thermal fatigue life of a cylindrical shell, the strain range must be reduced. This may be accomplished by either reduction of the thermal load or reduction of the temperature gradient. The thermal load in many applications is difficult to reduce due to fixed process parameters. In this dissertation the thermal load is taken as a constraint and is held constant. The thermal gradient, on the other hand, can be reduced either by the selection of a high thermal conductivity material or by a thinner shell design. Copper has high thermal conductivity and could be used to decrease the temperature gradient, but it lacks strength and abrasion resistance and in some applications is susceptible to corrosion. A thinner shell design would also reduce the temperature gradient, but if too thin, the shell is subject to buckling and distortion which may be undesirable. To achieve a lower thermal gradient, dimensional stability, and abrasion resistance a three layered sandwich design is proposed. The multilayered cylinder will have inner and outer layers of high strength steel and a central layer of high conductivity copper. This design might be thought of as the thermal equivalent of the mechanical "I-beam." The inside and outside layers of steel are used to give strength, stiffness, stability, and abrasion resistance to the tube. The copper provides a high conductivity path for the heat flow. To the author's knowledge, no analytical technique to determine and optimize the thermal fatigue life of a multilayered cylindrical shell has been developed. Such a technique will represent a significant contribution to the literature.

To determine the thermal fatigue life of a multilayered cylindrical shell, a numerical method using Mendelson's and Manson's technique³ and incorporating principles of incremental theory will be developed. It should be noted that total strain equations expressed in terms of temperature and plastic strain for a cylindrical tube, which are required for the Mendelson and Manson technique, have not appeared in the literature and will be derived in this dissertation. As part of the analysis, the radial temperature profile must be determined as a function of time, heat input, interface heat transfer coefficients, alloy thermal properties, and thicknesses of the layers. Equations for calculating the temperature profile in terms of these variables will be derived in this dissertation. The temperature profile will be used to perform an elastic-plastic stress analysis of the multilayered tube. Values from the stress analysis are used to determine the strain range and cyclic life of a design.

The optimization scheme allows the selection of a material or alloy for each layer, the layer thickness, inside and outside diameters, thermal load, and cycle times. The optimum design will be chosen by comparing the thermal fatigue life of several different designs that meet required constraints.

As a "demonstration" of the analysis and optimization method developed in this dissertation, a three layered tube will be optimized for a maximum thermal fatigue life for one set of constraints. The constraints imposed on the demonstration analysis are presented later in this dissertation and do not necessarily represent a real application.

II. THEORY AND DERIVATION OF HEAT FLOW AND STRAIN EQUATIONS

A numerical model that takes into account temperature dependent thermal and mechanical properties, strain hardening, and other material parameters that change due to thermomechanical cycling is desirable. However, this level of complexity is not necessary for optimizing composite tubing for thermal fatigue. A model that calculates the stresses and strains occurring in a design for any given thermal cycle could be used as a design tool. Once the strains are determined, a strain range could be calculated for each layer and used to determine the layer's life. Optimization occurs when the strain range in each layer is consistent with the maximum life of the tube as a whole. To establish a repeating strain range, a numerical model that couples a tube's thermal response to a stress analysis routine is required. The thermal part of such a model includes the following parameters:

- a. heat source temperature,
- b. heat transfer coefficients of the inside and outside diameter surfaces,
- c. thermophysical properties of the selected materials, such as thermal conductivity, density, and specific heat,
- d. layer thicknesses, and

- e. the duration of the heating and cooling phases of a thermal cycle.

The stress analysis takes into account both the elastic and plastic nature of the composite's response as a function of temperature during cyclic heating and cooling.

Development of equations for radial temperature and stress distribution in each layer requires that certain boundary conditions must be met at surfaces and interfaces. Once developed, the equations are implemented into a thermo-elastic-plastic model of a three layered steel-copper-steel composite tube, and the model is used to optimize the thermal fatigue life of the tube with certain thermal and physical constraints. This analysis assumes a specified inner radius, with a heat input, three layers of total thickness, and a water cooled outer surface.

Derivation of Finite Difference Heat Flow Equations

To determine the temperature profile in a three layered composite tube, a finite difference solution to transient heat flow is required. There are many texts on the finite difference solution to heat flow; the following equations have been derived based on the physical formulation techniques described by Myers.⁷

The finite difference technique requires that the tube be divided into many small layers (nodes) such that heat balance equations may be written for each layer (node). The nodes are subscripted with i and j , where $r_{i,j}$ indicates the radial node at position i and time j . Figure 2 shows a general composite tube which consists of three layers of

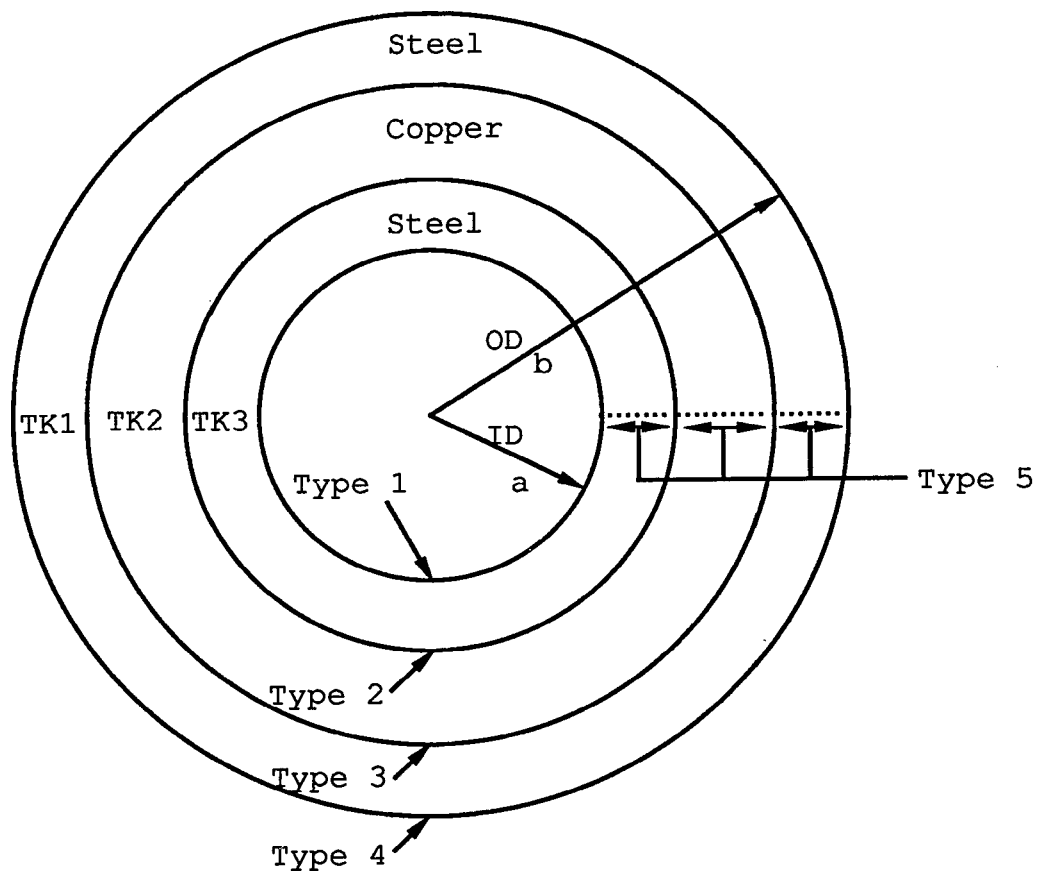


Figure 2. Drawing of a three layered cylindrical shell showing layer thicknesses, layer material, nodal system, and node types.

thickness TK1, TK2, and TK3. Each layer is subdivided into radial nodes which have different thermophysical properties based on its composition and temperature. Also notice that there are several different types of nodes, each of which require a different mathematical treatment. The node types are:

- (1) an inside diameter, ID, surface node which has associated with it a heat transfer coefficient, h_1 , which controls the rate of heat flow from the heat source into the tube,
- (2) an interface node between the steel and the copper alloy,
- (3) an interface node between the copper alloy and the steel,
- (4) an outside diameter, OD, surface node, which has associated with it a heat transfer coefficient, h_2 , which controls the rate of heat extraction from the tube, and
- (5) nodes that lie completely in the steel or completely in the copper alloy, but not at the interfaces.

Finite difference equations have been derived for each of these type nodes.

In the derivation of the finite difference equations, a one dimensional analysis has been used with geometric correction factors to account for the differences in area between nodal faces.

Shown in Figure 3 is the ID surface node; the heat balance equation for this node (node Type 1) may be written as:

$$q_{in} - q_{out} = q_{stored} \quad [1]$$

where q_{in} is heat flow into the node, q_{out} is heat flow out of the node, and q_{stored} is heat energy stored in the node due to a temperature change. Note that the heat balance equation is written about a control surface that is $\Delta r/2$ in the tube and $\Delta r/2$ in the heat source. Mathematically, q_{in} , q_{out} , and q_{stored} may be written as:

$$q_{in} = h_1 A_1 (T_{i,j} - T_{i+1,j}) \quad [2]$$

$$q_{out} = k A_2 \frac{(T_{i+1,j} - T_{i+2,j})}{\Delta r} \quad [3]$$

$$q_{stored} = \rho C_p \frac{A_1 + A_2}{2} \frac{\Delta r}{2} \frac{(T_{i+1,j+1} - T_{i+1,j})}{\delta t} \quad [4]$$

where h_1 is the heat transfer coefficient between the heat source and the inside surface of the tube, A_1 and A_2 are the areas of the node faces, subscripted T values are the temperatures at specific nodes and time steps, k is the thermal conductivity, Δr is the node thickness, ρ is the density, C_p is the specific heat, and δt is the time increment. Substituting equations [2], [3], and [4] into the heat balance equation [1] gives:

$$h_1 A_1 (T_{i,j} - T_{i+1,j}) - k A_2 \frac{(T_{i+1,j} - T_{i+2,j})}{\Delta r} = \rho C_p \frac{A_1 + A_2}{2} \frac{\Delta r}{2} \frac{(T_{i+1,j+1} - T_{i+1,j})}{\delta t} \quad [5]$$

Solving for the temperature of the surface node, $T_{i+1,j+1}$, at time $t+\delta t$ yields:

$$T_{i+1,j+1} = \frac{2h_1}{\rho C_p} \frac{2A_1}{A_1 + A_2} \frac{\delta t}{\Delta r} T_{i,j} +$$

$$\left[1 - \frac{2h_1}{\rho C_p} \frac{2A_1}{A_1 + A_2} \frac{\delta t}{\Delta r} - \frac{2k}{\rho C_p} \frac{2A_2}{A_1 + A_2} \frac{\delta t}{\Delta r^2} \right] T_{i+1,j} +$$

$$\frac{2k}{\rho C_p} \frac{2A_2}{A_1 + A_2} \frac{\delta t}{\Delta r^2} T_{i+2,j}$$
[6]

The terms containing areas A_1 and A_2 form geometric correction factors which can be simplified with respect to the radius, r . It is evident from Figure 4 that:

$$A_1 = A_{i+1} = r_{i+1} \theta z$$
[7]

and similarly:

$$A_2 = \frac{A_{i+1} + A_{i+2}}{2} = \frac{r_{i+1} \theta z + (r_{i+1} + \Delta r) \theta z}{2}$$
[8]

Letting GD_{i+1} be a geometric correction factor and substituting in the area equations produces:

$$GD_{i+1} = \frac{2A_1}{A_1 + A_2} = \frac{r_{i+1}}{r_{i+1} + \frac{\Delta r}{4}}$$
[9]

Similarly, another geometric correction factor is:

$$GF_{i+1} = \frac{2A_2}{A_1 + A_2}$$
[10]

and can be shown to be:

$$GF_{i+1} = \frac{r_{i+1} + \frac{\Delta r}{2}}{r_{i+1} + \frac{\Delta r}{4}}$$
[11]

Substituting these geometric factors into the node equation gives:

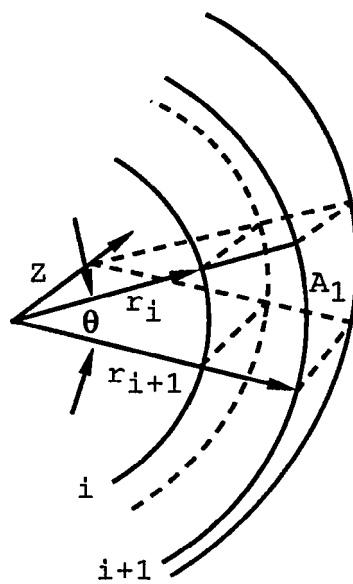


Figure 4. Nodal face of unit length in the z-direction.

$$\begin{aligned}
T_{i+1,j+1} &= \frac{2h_1}{\rho C_p} GD_{i+1} \frac{\delta t}{\Delta r} T_{i,j} + \\
&\left[1 - \frac{2h_1}{\rho C_p} GD_{i+1} \frac{\delta t}{\Delta r} - \frac{2k}{\rho C_p} GF_{i+1} \frac{\delta t}{\Delta r^2} \right] T_{i+1,j} + \\
&\frac{2k}{\rho C_p} GF_{i+1} \frac{\delta t}{\Delta r^2} T_{i+2,j}
\end{aligned} \tag{12}$$

Due to the uniqueness of the copper-steel interface (node Type 3), as shown in Figure 5, its solution is also presented. The heat balance equation may again be written as:

$$q_{in} - q_{out} = q_{stored} \tag{13}$$

where q_{in} is the heat flow into the node, q_{out} is the heat flow out of the node, and q_{stored} is the heat energy stored in the half copper-half steel node due to a temperature change. Note that the heat balance equation is written about a control surface that is $\Delta r/2$ in the copper and $\Delta r/2$ in the steel. Mathematically, q_{in} , q_{out} , and q_{stored} may be written as:

$$q_{in} = k_{Cu} A_1 \frac{(T_{i-1,j} - T_{i,j})}{\Delta r} \tag{14}$$

$$q_{out} = k_{St} A_3 \frac{(T_{i,j} - T_{i+1,j})}{\Delta r} \tag{15}$$

$$q_{stored} = (\rho_{St} C_p st + \rho_{Cu} C_p Cu) A_2 \frac{\Delta r}{2} \frac{(T_{i,j+1} - T_{i,j})}{\delta t} \tag{16}$$

where subscripted values of k , ρ , and C_p are used to distinguish between steel and copper properties. Substituting these equations into the heat balance equation gives:

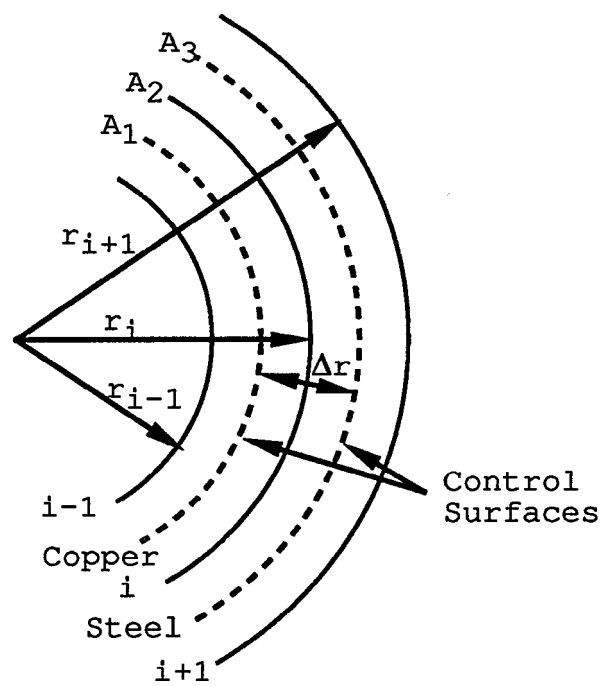


Figure 5. Plane view of copper-steel interface node.

$$k_{Cu} A_1 \frac{(T_{i-1,j} - T_{i,j})}{\Delta r} - k_{St} A_3 \frac{(T_{i,j} - T_{i+1,j})}{\Delta r} =$$

$$(\rho_{St} C_{p, St} + \rho_{Cu} C_{p, Cu}) A_2 \Delta r \frac{(T_{i,j+1} - T_{i,j})}{\delta t} \quad [17]$$

Defining α_1 and α_2 as:

$$\alpha_1 = \frac{k_{St}}{\rho_{St} C_{p, St} + \rho_{Cu} C_{p, Cu}} \quad [18]$$

$$\alpha_2 = \frac{k_{Cu}}{\rho_{St} C_{p, St} + \rho_{Cu} C_{p, Cu}} \quad [19]$$

and solving for $T_{i,j+1}$ yields:

$$T_{i,j+1} = 2\alpha_2 \left[\frac{2(A_{i-1} + A_i)}{A_i + A_{i-1} + A_{i+1}} \right] \frac{\delta t}{\Delta r} T_{i-1,j} +$$

$$\left(1 - 2\alpha_2 \left[\frac{2(A_{i-1} + A_i)}{2A_i + A_{i-1} + A_{i+1}} \right] \frac{\delta t}{\Delta r} - 2\alpha_1 \left[\frac{2(A_i + A_{i+1})}{2A_i + A_{i-1} + A_{i+1}} \right] \frac{\delta t}{\Delta r} \right) T_{i,j} +$$

$$2\alpha_1 \left[\frac{2(A_i + A_{i+1})}{2A_i + A_{i-1} + A_{i+1}} \right] \frac{\delta t}{\Delta r} T_{i+1,j} \quad [20]$$

which reduces to:

$$T_{i,j+1} = 2GB_i \alpha_2 \frac{\delta t}{\Delta r} T_{i-1,j} +$$

$$\left[1 - 2GB_i \alpha_2 \frac{\delta t}{\Delta r} - 2GA_i \alpha_1 \frac{\delta t}{\Delta r} \right] T_{i,j} +$$

$$2GA_i \alpha_1 \frac{\delta t}{\Delta r} T_{i+1,j} \quad [21]$$

where α_1 and α_2 are diffusivity factors and GA_i and GB_i are additional geometric correction factors.

The other node equations for node Types 2, 4, and 5 and their associated geometric correction factors are solved by

the same method. All equations and geometric correction factors are presented below for completeness.

Node Type 1 (the ID surface node):

$$\begin{aligned}
 T_{i+1,j+1} &= \frac{2h_1}{\rho C_p} GD_{i+1} \frac{\delta t}{\Delta r} T_{i,j} + \\
 &\left[1 - \frac{2h_1}{\rho C_p} GD_{i+1} \frac{\delta t}{\Delta r} - \frac{2k}{\rho C_p} GF_{i+1} \frac{\delta t}{\Delta r^2} \right] T_{i+1,j} + \\
 &\frac{2k}{\rho C_p} GF_{i+1} \frac{\delta t}{\Delta r^2} T_{i+2,j}
 \end{aligned} \tag{22}$$

Node Type 2 (the steel-copper interface node):

$$\begin{aligned}
 T_{i,j+1} &= 2GB_i \alpha_1 \frac{\delta t}{\Delta r^2} T_{i-1,j} + \\
 &\left[1 - 2GB_i \alpha_1 \frac{\delta t}{\Delta r^2} - 2GA_i \alpha_2 \frac{\delta t}{\Delta r^2} \right] T_{i,j} + \\
 &2GA_i \alpha_2 \frac{\delta t}{\Delta r^2} T_{i+1,j}
 \end{aligned} \tag{23}$$

Node Type 3 (the copper-steel interface node):

$$\begin{aligned}
 T_{i,j+1} &= 2GB_i \alpha_2 \frac{\delta t}{\Delta r^2} T_{i-1,j} + \\
 &\left[1 - 2GB_i \alpha_2 \frac{\delta t}{\Delta r^2} - 2GA_i \alpha_1 \frac{\delta t}{\Delta r^2} \right] T_{i,j} + \\
 &2GA_i \alpha_1 \frac{\delta t}{\Delta r^2} T_{i+1,j}
 \end{aligned} \tag{24}$$

Node Type 4 (the OD surface node):

$$T_{1,j+1} = 2GE_1 \alpha \frac{\delta t}{\Delta r^2} T_{1-1,j} +$$

$$\left[1 - 2GE_1 \alpha \frac{\delta t}{\Delta r^2} - \frac{2h_2}{\rho C_p} GC_i \frac{\delta t}{\Delta r} \right] T_{1,j} +$$

$$\frac{2h_2}{\rho C_p} GC_1 \frac{\delta t}{\Delta r} T_{1+1,j}$$
[25]

Node Type 5 (internal nodes of all steel or all copper):

$$T_{i,j+1} = GB_i \alpha \frac{\delta t}{\Delta r^2} T_{i-1,j} +$$

$$\left[1 - GB_i \alpha \frac{\delta t}{\Delta r^2} - GA_i \alpha \frac{\delta t}{\Delta r^2} \right] T_{i,j} +$$

$$GA_i \alpha \frac{\delta t}{\Delta r^2} T_{i+1,j}$$
[26]

Geometric correction factors are:

$$GA_i = \frac{r_i + \frac{\Delta r}{2}}{r_i}$$
[27]

$$GB_i = \frac{r_i - \frac{\Delta r}{2}}{r_i}$$
[28]

$$GC_i = \frac{r_i}{r_i + \frac{\Delta r}{4}}$$
[29]

$$GD_i = \frac{r_{i+1}}{r_{i+1} + \frac{\Delta r}{4}}$$
[30]

$$GE_i = \frac{r_i - \frac{\Delta r}{2}}{r_i - \frac{\Delta r}{4}}$$
[31]

$$GF_i = \frac{r_{i+1} + \frac{\Delta r}{2}}{r_{i+1} + \frac{\Delta r}{4}} \quad [32]$$

These equations have been implemented into the thermal section of the numerical model in latter sections of this dissertation.

Derivation of Strain Equations for a Cylindrical Tube

Before deriving equations for the stress analysis routine, it would be helpful to have definitions and a clear understanding of the different strain terms that appear in this dissertation.

Strain, of course, is a representation of the change in geometry of a solid from some initial to a final state. Linearized, infinitesimal strain is defined by the symmetric part of the displacement gradient. The change of geometry of a body can be accomplished by several means. Temperature change, mechanical load, and time dependent deformations are some of the causes of strain. A change in temperature of a body results in thermal strain. The amount of thermal strain is given by:

$$\epsilon_{\text{thermal}} = \alpha \Delta T \quad [33]$$

where α is the thermal expansion coefficient and ΔT is defined by the differences between the initial and final temperatures. If a body is heated nonuniformly or constrained by external forces, the strain consists of mechanical and thermal components. Mechanical strain components are related to stress. The mechanical strain can

have elastic and plastic parts. The sum of the mechanical and thermal strains is referred to, in this dissertation, as the total strain and is given by:

$$\epsilon_{\text{total}} = \epsilon_{\text{elastic}} + \epsilon_{\text{plastic}} + \epsilon_{\text{thermal}} \quad [34]$$

Since strain is a tensorial quantity it has principal components in the three orthogonal directions, usually designated by a subscript x, y, and z or r, θ , and z. For a cylindrical tube, as shown in Figure 6, the strain components (using a cylindrical coordinate system) are tangential, ϵ_{θ} , radial, ϵ_r , and axial, ϵ_z . These strains may be defined in terms of the displacements that occur when a tube is heated. Figure 7 shows a node of thickness dr that has undergone a displacement. The definition of tangential and radial strains are:

$$\epsilon_{\theta} = \frac{\text{Change in length}}{\text{Original length}} = \frac{2\pi(r+U) - 2\pi r}{2\pi r} = \frac{U}{r} \quad [35]$$

$$\epsilon_r = \frac{\text{Change in length}}{\text{Original length}} = \frac{(U + dU) - U}{dr} = \frac{dU}{dr} \quad [36]$$

The axial strain is defined as:

$$\epsilon_z = \frac{\text{Change in length}}{\text{Original length}} = \frac{dw}{dr} \quad [37]$$

where dw/dr is the gradient of the axial displacement field.

The Mendelson and Manson technique³ for the solution of the nonlinear differential equation that describes the thermomechanical response of a tube requires that total strain equations be derived from the equilibrium and compatibility equations that govern the geometry of the body in question. Their technique, with additions, has been used in the development of the numerical model in this dissertation.

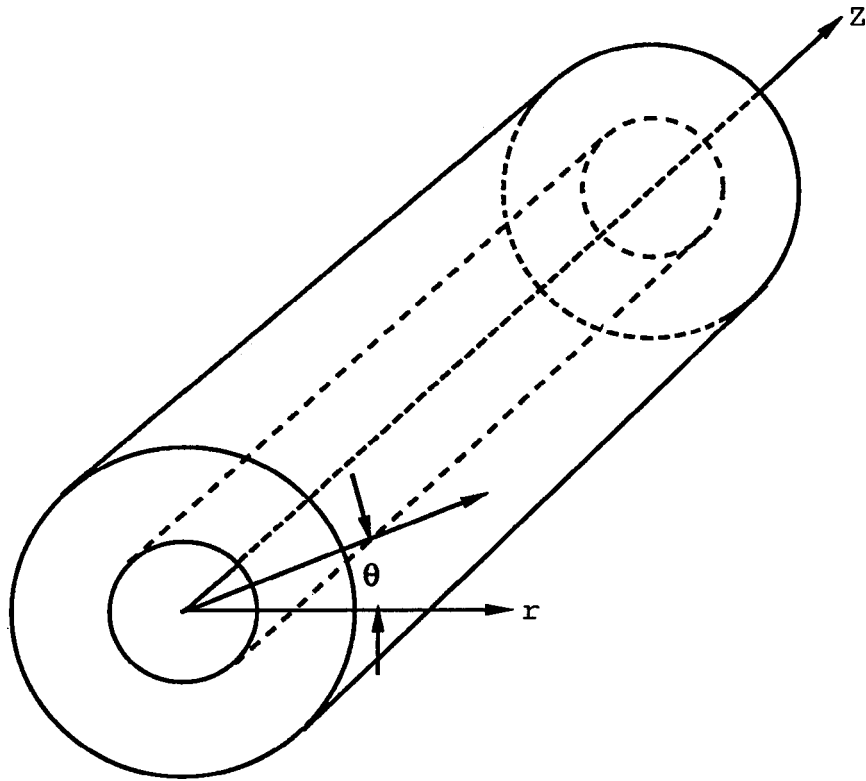
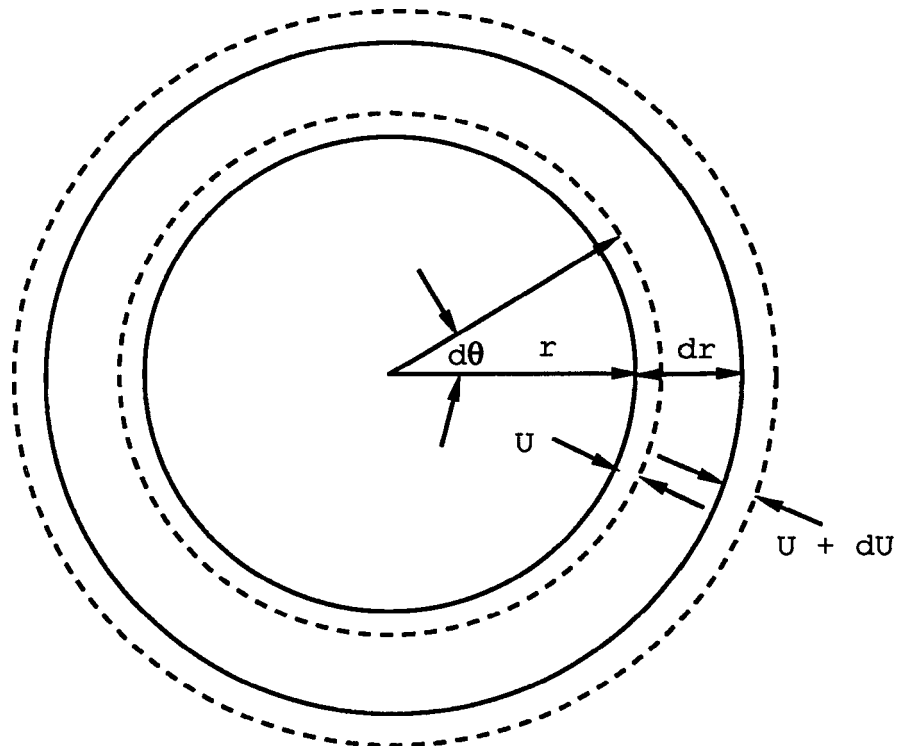


Figure 6. Section of a cylindrical tube showing cylindrical coordinate system.



$$\epsilon_{\theta} = \frac{U}{r}$$

$$\epsilon_r = \frac{dU}{dr}$$

Figure 7. A single radial node of radius, " r ," and thickness, " dr ," showing the radial displacements, U , $U+dU$, and the resulting strains.

Also required for their technique are equations that relate stress, strain, and plastic flow to a flow rule such as the von Mises criteria. Once these two steps are complete the equations are applied according to incremental theory, in an iterative process, to calculate total and plastic strains which are used to calculate stresses. An incremental plasticity technique has been used because of its ability to treat unloading and reloading of stressed elements.

Figure 8 shows a free body diagram and force balance in terms of principal stresses: σ_r , σ_θ , and σ_z , for the unit volume differential element, $r \cdot d\theta \cdot dr \cdot dz$, where σ_r is the radial stress, σ_θ is the tangential or hoop stress, and σ_z is the stress in the axial direction. Due to symmetry, shearing stresses are zero and the tangential stress, σ_θ , is independent of the angle, theta. The sum of forces in the radial direction must be equal to zero to satisfy equilibrium, which results in:

$$\left[\sigma_r + \frac{d\sigma_r}{dr} dr \right] (r + dr) d\theta dz - \sigma_r r d\theta dz - 2\sigma_\theta dr dz \sin \frac{d\theta}{2} = 0 \quad [38]$$

$\sin d\theta/2$ is small and may be approximated by $d\theta/2$, which results in equation [38] simplifying to:

$$r \sigma_r + r \frac{d\sigma_r}{dr} dr + \sigma_r dr + \frac{d\sigma_r}{dr} (dr)^2 - r \sigma_r - \sigma_\theta dr = 0 \quad [39]$$

Neglecting higher order differential terms and rearranging results in:

$$\frac{d\sigma_r}{dr} + \frac{\sigma_r - \sigma_\theta}{r} = 0 \quad [40]$$

which is the equilibrium equation for the radial direction.

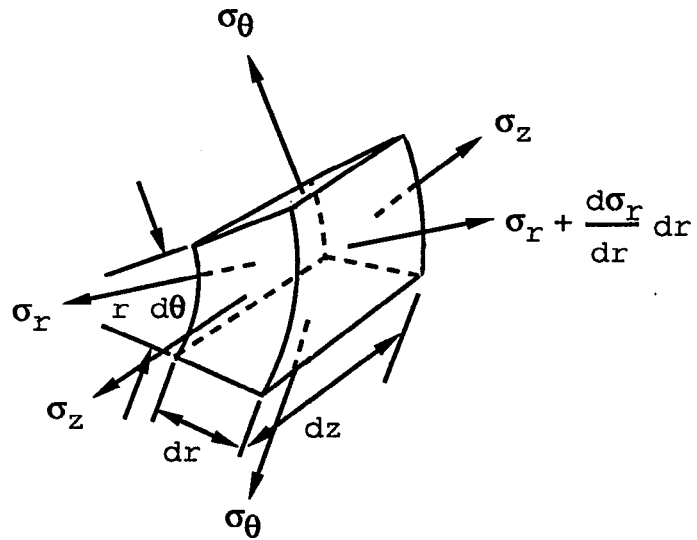


Figure 8. Free body diagram showing forces acting on differential element of tube.

Equilibrium also requires that the sum of the forces from any internal or external pressure acting on the tube must balance. Figure 9 shows a free body diagram of a half section of a tube with internal and external pressures acting on it. The length of the tube under consideration is unity. The y-component of force, per unit length, due to a pressure on a small surface area of the ID may be written as:

$$F_{y_i} = \Delta F_{p_i} \sin \theta = p_i (r_i \Delta \theta) \sin \theta \quad [41]$$

where F_{y_i} is the component of force in the y-direction, ΔF_{p_i} is the force on a small element of the ID surface due to an inside pressure, p_i , at inside radius, r_i . Similarly, for the external pressure:

$$F_{y_o} = \Delta F_{p_o} \sin \theta = p_o (r_o \Delta \theta) \sin \theta \quad [42]$$

where F_{y_o} is the component of force in the y-direction and ΔF_{p_o} is the force on a small element of the OD surface due to the external pressure, p_o , at outside radius r_o . The force, per unit length, connecting the two half sections may be written as:

$$F_{\theta} = 2 \sum \sigma_{\theta} \Delta r \quad [43]$$

Taking the limit as $\Delta \theta$ and Δr approach zero and summing the forces in the y-direction yields:

$$\int_0^{\pi} p_i r_i \sin \theta d\theta - \int_0^{\pi} p_o r_o \sin \theta d\theta = 2 \int_a^b \sigma_{\theta} dr \quad [44]$$

Integrating results in:

$$p_i r_i - p_o r_o = \int_a^b \sigma_{\theta} dr \quad [45]$$

Now equating the pressures p_i and p_o to zero, for the case under consideration, one obtains:

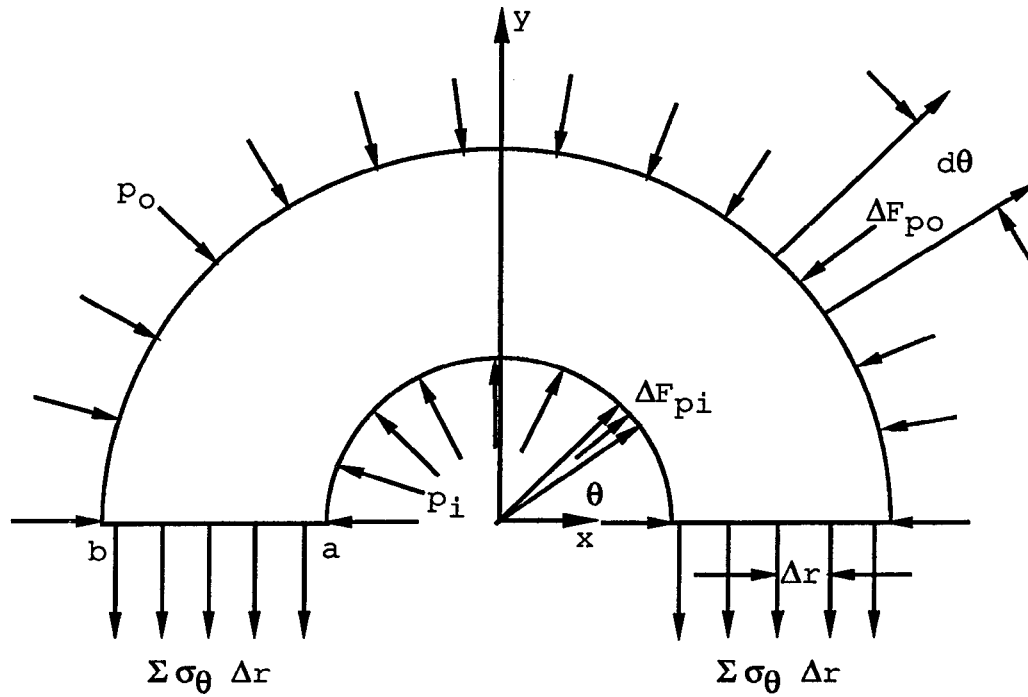


Figure 9. Free body diagram of a half section of a tube showing forces acting in the y -direction. The inside radius is "a" and the outside radius is "b." The inside pressure is p_i and the outside pressure is p_o .

$$\int_a^b \sigma_\theta \, dr = 0 \quad [46]$$

Two special cases arise when considering forces in the z-direction. The first case is that of plane strain where the net strain is equal to zero. This requires that a restraining force be applied to the end faces of the tube such that the strain in the z-direction is constant and equal to zero. The other case of plane strain occurs when the sum of forces in the z-direction are equal to zero. This condition states that a σ_z distribution exists across the tube wall such that a plane section taken through the tube, normal to the axial direction, will remain plane during thermal cycling; that is, no telescoping occurs between layers in the composite and ϵ_z is constant and independent of r and θ . Other conditions that must be satisfied for the analysis are those of compatibility and boundary conditions on the ID and OD surfaces. Compatibility is a condition of continuity of strain in the theta direction between two adjacent elements in the tube. This condition may be expressed as:

$$\epsilon_r = r \frac{d\epsilon_\theta}{dr} + \epsilon_\theta \quad [47]$$

where ϵ_r and ϵ_θ are the radial and tangential components of total strain. A free surface cannot support a radial stress, so this leads to an ID and OD boundary condition given as:

$$\sigma_r = 0$$

at radius = a

and
$$\sigma_r = 0$$

at radius = b

where a and b are the inside and outside radii of the tube.

From the above equations and conditions, it is desirable to solve for the radial displacement, U . Once U is obtained, ϵ_θ and ϵ_r are defined by equations [35] and [36], respectively. Using total strain equations [48], [49], and [50], which include elastic, thermal, and plastic components:

$$\epsilon_r = \frac{1}{E} \left[\sigma_r - \mu(\sigma_\theta + \sigma_z) \right] + \alpha T + \epsilon_{rp} \quad [48]$$

$$\epsilon_\theta = \frac{1}{E} \left[\sigma_\theta - \mu(\sigma_r + \sigma_z) \right] + \alpha T + \epsilon_{\theta p} \quad [49]$$

$$\epsilon_z = \frac{1}{E} \left[\sigma_z - \mu(\sigma_r + \sigma_\theta) \right] + \alpha T - (\epsilon_{rp} + \epsilon_{\theta p}) \quad [50]$$

where E is elastic modulus, μ is Poisson's ratio, α is the thermal expansion coefficient (not to be confused with the thermal diffusivities α_1 and α_2), and ϵ_{rp} and $\epsilon_{\theta p}$ are the radial and tangential components of plastic strain, it can be shown that:

$$\sigma_r = \lambda (\epsilon_r + \epsilon_\theta + \epsilon_z - 3\alpha T) + 2G (\epsilon_r - \alpha T - \epsilon_{rp}) \quad [51]$$

$$\sigma_\theta = \lambda (\epsilon_r + \epsilon_\theta + \epsilon_z - 3\alpha T) + 2G (\epsilon_\theta - \alpha T - \epsilon_{\theta p}) \quad [52]$$

$$\sigma_z = \lambda (\epsilon_r + \epsilon_\theta + \epsilon_z - 3\alpha T) + 2G (\epsilon_z - \alpha T + \epsilon_{rp} + \epsilon_{\theta p}) \quad [53]$$

where λ and G are known as Lamé's constants and are given by:

$$\lambda = \frac{\mu E}{(1 + \mu)(1 - 2\mu)} \quad [54]$$

$$G = \frac{E}{2(1 + \mu)} \quad [55]$$

Substituting σ_r and σ_θ into the radial equilibrium equation, letting E , μ , and α be constant, using the compatibility relation to express ϵ_r in terms of ϵ_θ , and rearranging gives:

$$\frac{d}{dr} \left[\frac{1}{r} \frac{d}{dr} (r^2 \epsilon_{\theta}) \right] = \frac{d}{dr} \left[\frac{1 + \mu}{1 - \mu} \alpha T + \frac{1 - 2\mu}{1 - \mu} \epsilon_{rp} \right] + \frac{1 - 2\mu}{1 - \mu} \left[\frac{\epsilon_{rp} - \epsilon_{\theta p}}{r} \right] \quad [56]$$

which is a second order differential equation. Substituting U/r for ϵ_{θ} yields:

$$\frac{d}{dr} \left[\frac{1}{r} \frac{d}{dr} (rU) \right] = \frac{d}{dr} \left[\frac{1 + \mu}{1 - \mu} \alpha T + \frac{1 - 2\mu}{1 - \mu} \epsilon_{rp} \right] + \frac{1 - 2\mu}{1 - \mu} \left[\frac{\epsilon_{rp} - \epsilon_{\theta p}}{r} \right] \quad [57]$$

which can be solved for the displacement, U , in terms of temperature and plastic strain. The left-hand side of the above equation is an exact differential and may be solved by integration. Integration of both sides gives:

$$\frac{1}{r} \frac{d}{dr} (rU) = \frac{1 + \mu}{1 - \mu} \alpha T + \frac{1 - 2\mu}{1 - \mu} \epsilon_{rp} + \frac{1 - 2\mu}{1 - \mu} \int_a^r \frac{(\epsilon_{rp} - \epsilon_{\theta p})}{r} dr + 2C_1 \quad [58]$$

where C_1 is a constant of integration. Multiplying both sides by r and integrating again results in:

$$(rU) = \frac{1 + \mu}{1 - \mu} \int_a^r \alpha T r dr + \frac{1 - 2\mu}{1 - \mu} \int_a^r \epsilon_{rp} r dr + \frac{1 - 2\mu}{1 - \mu} \int_a^r r \int_a^r \frac{(\epsilon_{rp} - \epsilon_{\theta p})}{r} dr dr + C_1 r^2 + C_2 \quad [59]$$

where C_2 is a constant of integration. Now dividing both sides by r gives:

$$\begin{aligned}
U = & \frac{1 + \mu}{1 - \mu} \frac{1}{r} \int_a^r \alpha T r \, dr + \frac{1 - 2\mu}{1 - \mu} \frac{1}{r} \int_a^r \epsilon_{rp} r \, dr + \\
& \frac{1 - 2\mu}{1 - \mu} \frac{1}{r} \int_a^r r \int_a^r \frac{(\epsilon_{rp} - \epsilon_{\theta p})}{r} \, dr \, dr + C_1 r + \frac{C_2}{r}
\end{aligned} \tag{60}$$

The double integral may be simplified by applying the integration by parts theorem. Recall that:

$$\int u \, dv = uv - \int v \, du \tag{61}$$

By letting:

$$u = \int \frac{\epsilon_{rp} - \epsilon_{\theta p}}{r} \, dr \tag{62}$$

du becomes:

$$du = \frac{\epsilon_{rp} - \epsilon_{\theta p}}{r} \, dr \tag{63}$$

and letting:

$$dv = r \, dr \tag{64}$$

v becomes:

$$v = \frac{r^2}{2} \tag{65}$$

Substituting these into the integration by parts equation (equation [61]) results in the simplification of the double integral as shown below:

$$\frac{1 - 2\mu}{1 - \mu} \int_a^r r \int_a^r \frac{(\epsilon_{rp} - \epsilon_{\theta p})}{r} \, dr \, dr =$$

$$\frac{1 - 2\mu}{2(1 - \mu)} \left[r^2 \int_a^r \frac{(\epsilon_{rp} - \epsilon_{\theta p})}{r} dr - \int_a^r (\epsilon_{rp} - \epsilon_{\theta p}) r dr \right] \quad [66]$$

Substituting this simplification into equation [60] and rearranging gives:

$$U = \frac{1 + \mu}{1 - \mu} \frac{1}{r} \int_a^r \alpha T r dr + \frac{1 - 2\mu}{2(1 - \mu)} \frac{1}{r} \int_a^r (\epsilon_{rp} + \epsilon_{\theta p}) r dr + \frac{1 - 2\mu}{2(1 - \mu)} \frac{1}{r} \int_a^r \frac{(\epsilon_{rp} - \epsilon_{\theta p})}{r} dr + C_1 r + \frac{C_2}{r} \quad [67]$$

Now that one has an expression for U , ϵ_{θ} is obtained by dividing U by r and ϵ_r is obtained by differentiating U with respect to r , which results in the following equations.

$$\epsilon_{\theta} = \frac{1 + \mu}{1 - \mu} \frac{1}{r^2} \int_a^r \alpha T r dr + \frac{1 - 2\mu}{2(1 - \mu)} \frac{1}{r^2} \int_a^r (\epsilon_{rp} + \epsilon_{\theta p}) r dr + \frac{1 - 2\mu}{2(1 - \mu)} \frac{1}{r^2} \int_a^r \frac{(\epsilon_{rp} - \epsilon_{\theta p})}{r} dr + C_1 + \frac{C_2}{r^2} \quad [68]$$

$$\epsilon_r = -\epsilon_{\theta} + \frac{1 + \mu}{1 - \mu} \alpha T + \frac{1 - 2\mu}{(1 - \mu)} \epsilon_{rp} + \frac{1 - 2\mu}{(1 - \mu)} \int_a^r \frac{(\epsilon_{rp} - \epsilon_{\theta p})}{r} dr + 2C_1 \quad [69]$$

Now applying the plane strain condition where the axial force on the end faces is zero states that:

$$\int_0^{2\pi} \int_a^b \sigma_z r dr d\theta = 0 \quad [70]$$

which reduces to:

$$\int_a^b \sigma_z r dr = 0 \quad [71]$$

Substituting ϵ_r and ϵ_θ into σ_z , equation [53], integrating as shown in equation [71], and solving for ϵ_z gives:

$$\begin{aligned} \epsilon_z = & - \frac{(2 - \mu)(1 - 2\mu)}{(1 - \mu)^2 (b^2 - a^2)} \int_a^b (\epsilon_{rp} + \epsilon_{\theta p}) r dr + \\ & \frac{2(1 + \mu)(1 - 2\mu)}{(1 - \mu)^2 (b^2 - a^2)} \int_a^b \alpha T r dr - \\ & \frac{\mu(1 - 2\mu)}{(1 - \mu)^2} \int_a^b \frac{\epsilon_{rp} - \epsilon_{\theta p}}{r} dr - \frac{2\mu}{1 - \mu} C_1 \end{aligned} \quad [72]$$

Using the ID and OD boundary conditions, the radial stress equation, ϵ_r , and ϵ_θ enables one to solve for the constants of integration C_1 and C_2 . Substituting ϵ_θ and ϵ_r (equations [68] and [69], respectively) into the radial stress equation [51] and evaluating the integrals at r equals to "a" for the ID boundary condition yields:

$$\begin{aligned} \sigma_r = 0 = \lambda & \left[\frac{1 + \mu}{1 - \mu} \alpha T + \frac{1 - 2\mu}{1 - \mu} \epsilon_{rp} + 2 C_1 + \epsilon_z - 3 \alpha T \right] + \\ & 2 G \left[\frac{1 + \mu}{1 - \mu} \alpha T + \frac{1 - 2\mu}{1 - \mu} \epsilon_{rp} + C_1 - \frac{C_2}{a^2} - \alpha T - \epsilon_{rp} \right] \end{aligned} \quad [73]$$

Solving for C_1 in terms of C_2 and ϵ_z gives:

$$C_1 = \frac{1 - 2\mu}{a^2} C_2 - \mu \epsilon_z \quad [74]$$

Substituting ϵ_θ and ϵ_r (equations [68] and [69], respectively) into the radial stress equation [51] and

evaluating the integrals at r equals to "b" for the OD boundary condition yields:

$$\begin{aligned}
\sigma_r = 0 = & \lambda \left[\frac{1 + \mu}{1 - \mu} \alpha T + \frac{1 - 2\mu}{1 - \mu} \epsilon_{rp} \right] + \\
& \lambda \left[\frac{1 - 2\mu}{1 - \mu} \int_a^b \frac{(\epsilon_{rp} - \epsilon_{\theta p})}{r} dr + 2 C_1 + \epsilon_z - 3 \alpha T \right] + \\
2G \left[- \frac{1 + \mu}{1 - \mu} \frac{1}{b^2} \int_a^b \alpha T r dr + \frac{1 - 2\mu}{2(1 - \mu)} \frac{1}{b^2} \int_a^b (\epsilon_{rp} + \epsilon_{\theta p}) r dr \right] + \\
2G \left[\frac{1 - 2\mu}{2(1 - \mu)} \int_a^b \frac{(\epsilon_{rp} - \epsilon_{\theta p})}{r} dr + \frac{1 + \mu}{1 - \mu} \alpha T + \frac{1 + 2\mu}{1 - \mu} \epsilon_{rp} \right] + \\
& 2G \left[C_1 + \frac{C_2}{b^2} - \alpha T - \epsilon_{rp} \right] \tag{75}
\end{aligned}$$

By multiplying equation [73] by -1 and adding it to equation [75] C_1 and ϵ_z are eliminated and a solution for C_2 is obtained. Upon substituting C_1 and C_2 into the strain equations and simplifying ϵ_r , ϵ_{θ} , and ϵ_z become:

$$\begin{aligned}
\epsilon_{\theta} = & \frac{1 + \mu}{1 - \mu} \frac{1}{r^2} \int_a^r \alpha T r dr + \frac{1 - 2\mu}{2(1 - \mu)} \frac{1}{r^2} \int_a^r (\epsilon_{rp} + \epsilon_{\theta p}) r dr + \\
& \frac{1 - 2\mu}{2(1 - \mu)} \frac{1}{r^2} \int_a^r \frac{(\epsilon_{rp} - \epsilon_{\theta p})}{r} dr + C_1 + \frac{C_2}{r^2} \tag{76}
\end{aligned}$$

$$\epsilon_r = - \epsilon_{\theta} + \frac{1 + \mu}{1 - \mu} \alpha T + \frac{1 - 2\mu}{(1 - \mu)} \epsilon_{rp} +$$

$$\frac{1 - 2\mu}{(1 - \mu)} \int_a^r \frac{(\epsilon_{rp} - \epsilon_{\theta p})}{r} dr + 2C_1 \quad [77]$$

$$\epsilon_z = \frac{2}{b^2 - a^2} \left[\int_a^b \alpha T r dr - \int_a^b (\epsilon_{rp} + \epsilon_{\theta p}) r dr \right] + \frac{\mu a^2}{(1 - \mu^2)(b^2 - a^2)} \int_a^b \frac{(\epsilon_{rp} - \epsilon_{\theta p})}{r} dr \quad [78]$$

$$C_1 = \frac{1 - 2\mu}{a^2} C_2 - \mu \epsilon_z \quad [79]$$

$$C_2 = \frac{1 + \mu}{1 - \mu} \frac{a^2}{(b^2 - a^2)} \int_a^b \alpha T r dr - \frac{a^2 b^2}{2(1 - \mu)(b^2 - a^2)} \int_a^b \frac{(\epsilon_{rp} - \epsilon_{\theta p})}{r} dr + \frac{(1 - 2\mu)a^2}{2(1 - \mu)(b^2 - a^2)} \int_a^b (\epsilon_{rp} + \epsilon_{\theta p}) r dr \quad [80]$$

Once the strains are calculated, stresses may be obtained from the general stress equations [51], [52], and [53].

Next, it is necessary to have a reference stress-strain behavior and a flow rule which applies the stress-strain function to states of strain other than the referred test. The tension test is the reference test, the von Mises criteria are the criteria for the change of stress state. The von Mises criteria are implemented by developing equations that relate the total strains, ϵ_r , ϵ_θ , and ϵ_z , to

the elastic and plastic strains as measured in a uniaxial tensile test. This relationship is established through the concept of equivalent stress and equivalent plastic strain as developed by von Mises⁸ and the equivalent total strain as given by Manson.⁹ These stresses and strains are obtained from the following equations:

$$\sigma_e = \frac{1}{\sqrt{2}} \sqrt{(\sigma_r - \sigma_\theta)^2 + (\sigma_r - \sigma_z)^2 + (\sigma_\theta - \sigma_z)^2} \quad [81]$$

$$\epsilon_{et} = \frac{\sqrt{2}}{3} \sqrt{(\epsilon_r - \epsilon_\theta)^2 + (\epsilon_r - \epsilon_z)^2 + (\epsilon_\theta - \epsilon_z)^2} \quad [82]$$

$$\epsilon_{ep} = \frac{\sqrt{2}}{3} \sqrt{(\epsilon_{rp} - \epsilon_{\theta p})^2 + (\epsilon_{rp} - \epsilon_{zp})^2 + (\epsilon_{\theta p} - \epsilon_{zp})^2} \quad [83]$$

where σ_e is the equivalent stress, ϵ_{et} is the equivalent total strain, and ϵ_{ep} is the equivalent plastic strain. The thermal strains are included in the total strains, ϵ_r , ϵ_θ , and ϵ_z . Because of assumed isotropy of thermal expansion, the components of thermal strain are equal to each other and when substituted into the equivalent total strain equation (equation [82]) their contribution to the equivalent total strain is zero. The equivalent stress is synonymous with the axial normal stress from a uniaxial tensile test. The equivalent total strain can be divided into equivalent elastic and equivalent plastic strains by equation [84].¹⁰

$$\epsilon_{et} = \epsilon_{ep} + \frac{2(1 + \mu)}{3} \frac{\sigma_e}{E} \quad [84]$$

A uniaxial stress strain curve may now be used to determine the relationship between equivalent elastic plus plastic strain and equivalent plastic strain for a material at various temperatures. Note that the definitions in equations

[81] through [84] define positive definite scalar quantities. They cannot be negative nor do they have directionality or coordinate components.

Figure 10 shows a typical stress-strain curve from which ϵ_{et} and ϵ_{ep} data may be taken. By taking several points of data a plot of ϵ_{et} vs. ϵ_{ep} may be made as shown in Figure 11. The relationship between the two strains is nearly linear and may be represented by a linear equation. Curve fitting gives an equation of the form:

$$\epsilon_{ep} = a + b \epsilon_{et} \quad [85]$$

where the intercept, a , is negative and relates to the elasticity of a material and the slope, b , represents a strain hardening factor. It should be evident that if the calculated value of ϵ_{ep} is negative, the strain of the node under evaluation is in the elastic domain and if ϵ_{ep} is positive, plastic flow occurs.

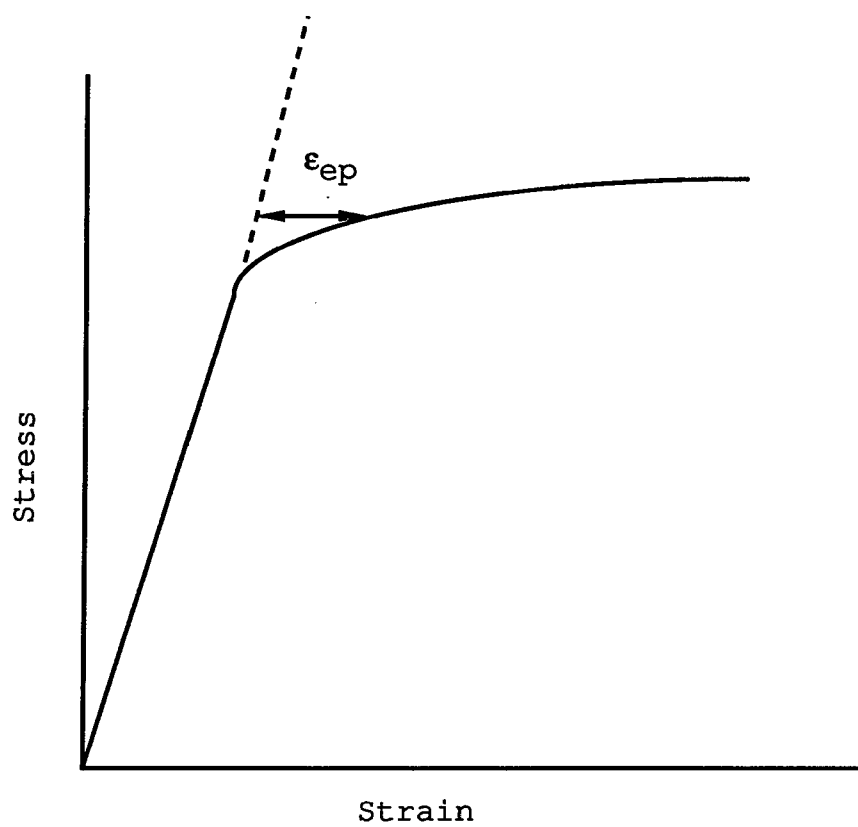
Once a positive equivalent plastic strain is calculated the components of plastic strain, ϵ_{rp} , $\epsilon_{\theta p}$, and ϵ_{zp} , may be determined by equations [86], [87], and [88].¹¹

$$\epsilon_{rp} = \frac{1}{3} \frac{\epsilon_{ep}}{\epsilon_{et}} \left[2\epsilon_r - \epsilon_{\theta} - \epsilon_z \right] \quad [86]$$

$$\epsilon_{\theta p} = \frac{1}{3} \frac{\epsilon_{ep}}{\epsilon_{et}} \left[2\epsilon_{\theta} - \epsilon_r - \epsilon_z \right] \quad [87]$$

$$\epsilon_{zp} = \frac{1}{3} \frac{\epsilon_{ep}}{\epsilon_{et}} \left[2\epsilon_z - \epsilon_r - \epsilon_{\theta} \right] \quad [88]$$

With equation [82] and equations [84] through [88], one can now describe a material's thermomechanical behavior, provided that tensile test data as a function of temperature are



$$\epsilon_{et} = \frac{2(1 + \mu)}{3} \frac{\sigma_e}{E} + \epsilon_{ep}$$

Figure 10. Stress-strain curve of a typical steel showing the relationship between equivalent plastic and equivalent total strain.

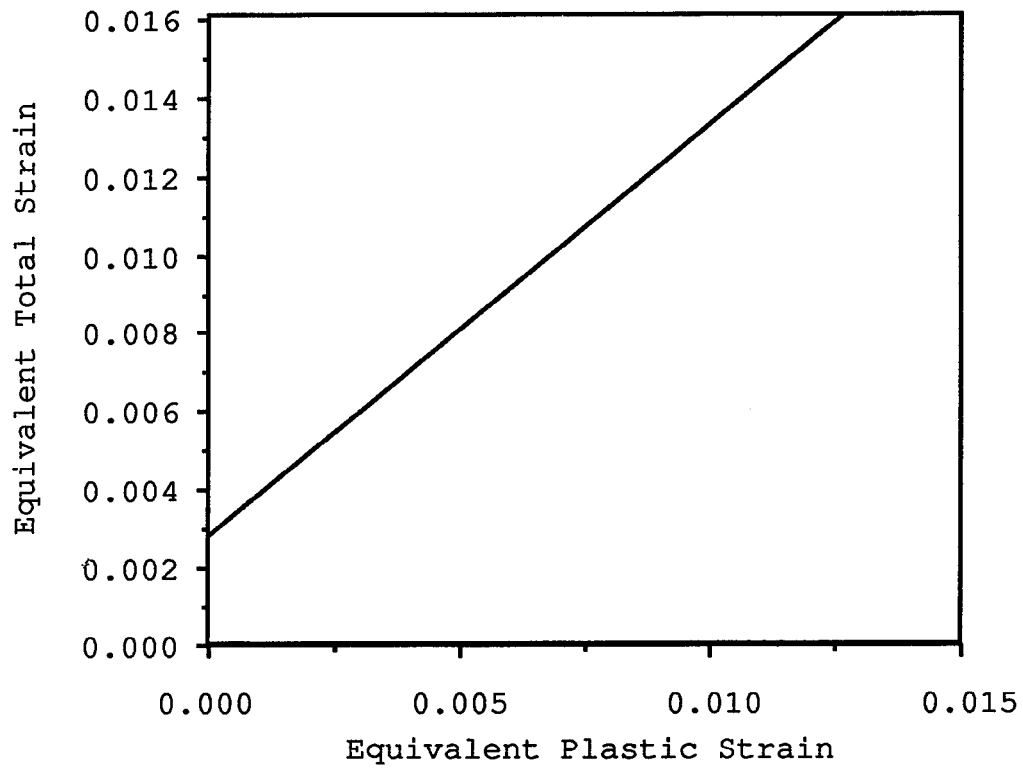


Figure 11. Equivalent total and equivalent plastic strain relationship for a typical steel obtained from stress-strain data at room temperature.

available. An iterative process may be followed whereby total strains and plastic strains, in the coordinate components, are calculated that satisfy conditions of equilibrium, compatibility, and the thermomechanical behavior of a material.

III. IMPLEMENTATION OF HEAT FLOW AND STRAIN EQUATIONS INTO A THERMO-ELASTIC-PLASTIC NUMERICAL MODEL

For numerical values of stress and strain to be calculated for a particular composite tube design under a thermal load, the heat flow and total strain equations developed in the previous section must be incorporated into a numerical model.

The implementation of the finite difference equations to calculate the temperature profile in the tube is accomplished via a computer program. The logic explaining the implementation of these equations is best understood by the step-by-step description given in Table 1.

Due to the transient heat flow and the unloading that occurs for the design under investigation, the total strain equations developed in the previous section have been implemented in the numerical model using the incremental theory of plasticity. This theory suggests that the loading cycle be divided into small load increments so that the plastic strain for each node may be followed to detect when unloading occurs. When unloading, the peak value of plastic strain is held constant until additional loading results in a plastic strain above the peak value or a plastic strain occurs in the opposite direction.

This technique requires that the plastic strains as seen in the strain equations be divided into two parts. The first

Table 1
Temperature Profile Calculations

Step Number	Description of Procedure
1.	Select a node thickness, Δr , and time increment, δt , such that temperature calculations result in stable values. It has been shown by Rohsenow, Hartnett, and Ganic ¹² that this condition occurs if the nodal thickness and time increment satisfy the following criteria:
	$\delta t \leq \frac{1}{2} \frac{(\Delta r)^2}{\alpha}$
	where α is the diffusivity of the copper alloy. A 0.5 mm node thickness and a 0.002 second time increment was used in this dissertation.
2.	Set up nodal spacing across the wall of the tube so that nodes fall on the two steel-copper interfaces and the ID and OD surfaces.
3.	Calculate geometric correction factors for each node, using equations [27], [28], [29], [30], [31], and [32].
4.	Initialize all node temperatures to initial temperature of 25 C.
5.	Initialize time to zero.
6.	Set heat source temperature to 900 C (i.e., $T_{i=0,j}$ in ID node equation [22]).
7.	Increment time by one time step: $\text{time} = \text{time} + \delta t.$
8.	Calculate the temperature, $T_{i,j+1}$, for each node using finite difference equations [22], [23], [24], [25], and [26].
9.	Set $T_{i,j}$ equal to $T_{i,j+1}$ for all nodes. This sets the temperature of each node to the calculated temperature for the next time increment.
10.	Check time to determine if stress analysis is to be performed. If so, call stress analysis routine; if not, continue.
11.	Check temperature of OD node to determine if heat transfer coefficient needs to be changed.
12.	Check time to determine if heat source temperature is to be reset to room temperature. If "no" go to step 6. If "yes" set temperature of zeroth node to room temperature and go to step 7.
13.	Check time to determine if cycle is complete; if complete reset time to zero and go to step 6. If not complete, continue.
14.	Repeat procedure until desired number of cycles have been completed.

are the plastic strains that occur before the current load increment, which are denoted as ϵ_{rp} and/or $\epsilon_{\theta p}$, while the second are those for the current load increment, which are denoted as $\Delta\epsilon_{rp}$ and/or $\Delta\epsilon_{\theta p}$. Introducing these changes into the total strain equation allows equations [76] through [80] to be rewritten as shown below.

$$\begin{aligned} \epsilon_{\theta} = & \frac{1 + \mu}{1 - \mu} \frac{1}{r^2} \int_a^r \alpha T r dr + \\ & \frac{1 - 2\mu}{2(1 - \mu)} \frac{1}{r^2} \int_a^r (\epsilon_{rp} + \epsilon_{\theta p} + \Delta\epsilon_{rp} + \Delta\epsilon_{\theta p}) r dr + \\ & \frac{1 - 2\mu}{2(1 - \mu)} \frac{1}{r^2} \int_a^r \frac{(\epsilon_{rp} - \epsilon_{\theta p} + \Delta\epsilon_{rp} - \Delta\epsilon_{\theta p})}{r} dr + C_1 + \frac{C_2}{r^2} \end{aligned} \quad [89]$$

$$\begin{aligned} \epsilon_r = & -\epsilon_{\theta} + \frac{1 + \mu}{1 - \mu} \alpha T + \frac{1 - 2\mu}{(1 - \mu)} (\epsilon_{rp} + \Delta\epsilon_{rp}) + \\ & \frac{1 - 2\mu}{(1 - \mu)} \int_a^r \frac{(\epsilon_{rp} - \epsilon_{\theta p} + \Delta\epsilon_{rp} - \Delta\epsilon_{\theta p})}{r} dr + 2C_1 \end{aligned} \quad [90]$$

$$\begin{aligned} \epsilon_z = & \frac{2}{b^2 - a^2} \left[\int_a^b \alpha T r dr - \int_a^b (\epsilon_{rp} + \epsilon_{\theta p} + \Delta\epsilon_{rp} + \Delta\epsilon_{\theta p}) r dr \right] + \\ & \frac{\mu a^2}{(1 - \mu^2)(b^2 - a^2)} \int_a^b \frac{(\epsilon_{rp} - \epsilon_{\theta p} + \Delta\epsilon_{rp} - \Delta\epsilon_{\theta p})}{r} dr \end{aligned} \quad [91]$$

$$C_1 = \frac{1 - 2\mu}{a^2} C_2 - \mu \epsilon_z \quad [92]$$

$$C_2 = \frac{1 + \mu}{1 - \mu} \frac{a^2}{(b^2 - a^2)} \int_a^b \alpha T r dr -$$

$$\frac{a^2 b^2}{2 (1 - \mu) (b^2 - a^2)} \int_a^b \frac{(\epsilon_{rp} - \epsilon_{\theta p} + \Delta\epsilon_{rp} - \Delta\epsilon_{\theta p})}{r} dr +$$

$$\frac{(1 - 2\mu) a^2}{2 (1 - \mu) (b^2 - a^2)} \int_a^b (\epsilon_{rp} + \epsilon_{\theta p} + \Delta\epsilon_{rp} + \Delta\epsilon_{\theta p}) r dr \quad [93]$$

To calculate the increment of plastic strain occurring for the current load increment, the origin of the stress-strain curve must be shifted by the result of the prior plastic deformation. Remember that the equivalent stresses and strains are positive scalar quantities. This is accomplished by applying the following transformation equations to the strain values used in calculating the equivalent strains.

$$\epsilon_r^* = \epsilon_r - \Sigma \Delta \epsilon_{rp} \quad [94]$$

$$\epsilon_{\theta}^* = \epsilon_{\theta} - \Sigma \Delta \epsilon_{\theta p} \quad [95]$$

$$\epsilon_z^* = \epsilon_z - \Sigma \Delta \epsilon_{zp} \quad [96]$$

The summations in the above equations represent the sum of plastic strains increments occurring prior to the current load increment. Applying these transformations to the equivalent total strain and plastic strain component equations results in:

$$\epsilon_{et}^* = \frac{\sqrt{2}}{3} \sqrt{(\epsilon_r^* - \epsilon_{\theta}^*)^2 + (\epsilon_r^* - \epsilon_z^*)^2 + (\epsilon_{\theta}^* - \epsilon_z^*)^2} \quad [97]$$

$$\epsilon_{rp}^* = \frac{1}{3} \frac{\epsilon_{ep}}{\epsilon_{et}^*} \left[2\epsilon_r^* - \epsilon_{\theta}^* - \epsilon_z^* \right] \quad [98]$$

$$\epsilon_{\theta p}^* = \frac{1}{3} \frac{\epsilon_{ep}^*}{\epsilon_{et}^*} \left[2\epsilon_{\theta}^* - \epsilon_r^* - \epsilon_z^* \right] \quad [99]$$

$$\epsilon_{zp}^* = \frac{1}{3} \frac{\epsilon_{ep}^*}{\epsilon_{et}^*} \left[2\epsilon_z^* - \epsilon_r^* - \epsilon_{\theta}^* \right] \quad [100]$$

These transformations allow the equivalent total strain and plastic strain component equations to reflect only the strain occurring during the current load increment; the previous load increments having been accounted for by the summation of the plastic strains.

When going from the heating to the cooling phase of the thermal cycle, each node in turn reaches a peak equivalent total strain and begins to unload elastically. Nodes that have not deformed plastically unload along the same stress-strain line that they loaded on. Nodes that strained plastically unload along a line parallel to the original stress-strain line as shown in Figure 12. Nodes that yielded in the heating phase of the cycle are subject to high stresses of the opposite sign during the cooling phase and may yield in the opposite direction upon cooling. To determine if these nodes yield plastically during cooling, a new equivalent total strain reference is required. This reference is located at the point where the stress reversal (elastic unloading), for the node under consideration, occurs, and it has a unique value of ϵ_r , ϵ_{θ} , and ϵ_z from which the peak equivalent total strain is calculated. Using this shifted reference point, a new value of ϵ_{et} may be calculated to determine if plastic straining occurs during cooling. The

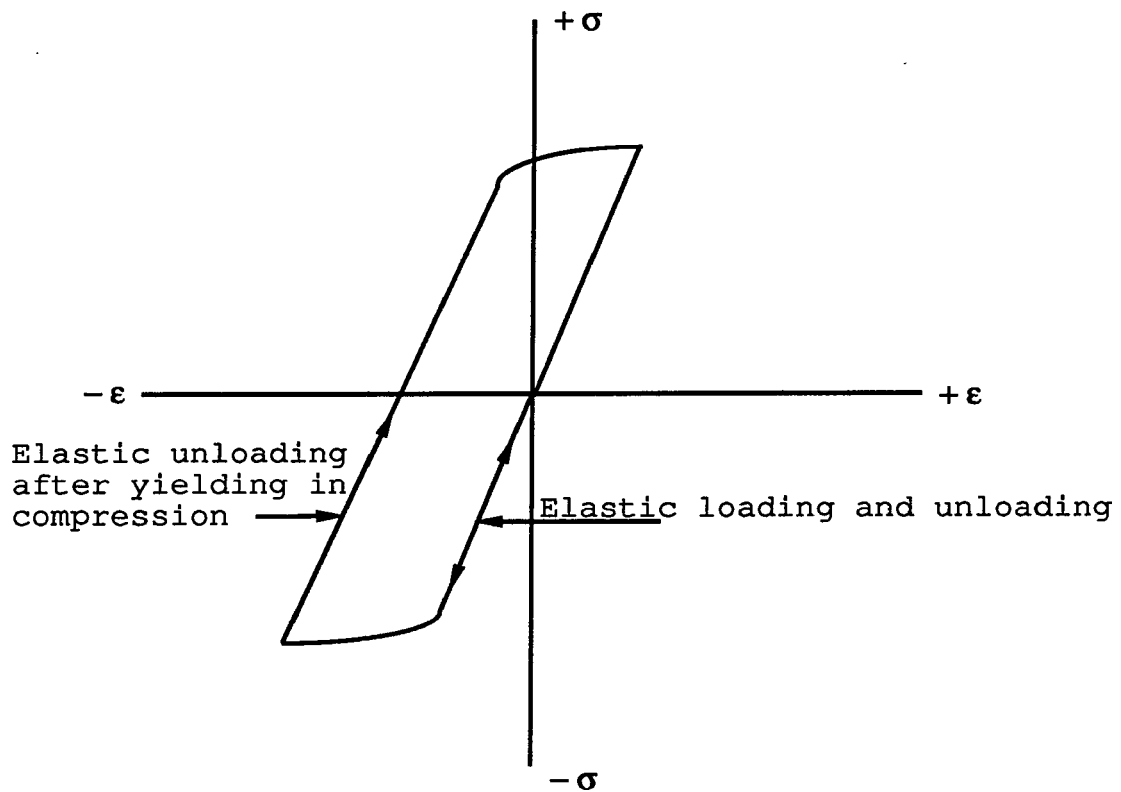


Figure 12. A hysteresis loop showing loading and unloading paths of nodes that undergo elastic and elastic-plastic deformation.

equivalent total strain, now calculated from the new reference point, is called the equivalent total strain star-star, ϵ_{et}^{**} . It may be determined by applying the following transformations to ϵ_r , ϵ_θ , and ϵ_z :

$$\epsilon_r^{**} = \epsilon_r - \epsilon_r^{pk} - \Sigma \Delta \epsilon_{rp} \quad [101]$$

$$\epsilon_\theta^{**} = \epsilon_\theta - \epsilon_\theta^{pk} - \Sigma \Delta \epsilon_{\theta p} \quad [102]$$

$$\epsilon_z^{**} = \epsilon_z - \epsilon_z^{pk} - \Sigma \Delta \epsilon_{zp} \quad [103]$$

where ϵ_r^{pk} , ϵ_θ^{pk} , and ϵ_z^{pk} are the unique values of ϵ_r , ϵ_θ , and ϵ_z that result in a peak value for ϵ_{et} as calculated by equation [82]. These transformations result in the ϵ_{et} equation becoming:

$$\epsilon_{et}^{**} = \frac{\sqrt{2}}{3} \sqrt{(\epsilon_r^{**} - \epsilon_\theta^{**})^2 + (\epsilon_r^{**} - \epsilon_z^{**})^2 + (\epsilon_\theta^{**} - \epsilon_z^{**})^2} \quad [104]$$

The relationship of the peak equivalent total strain, the equivalent total strain star-star, the equivalent plastic strain, and equivalent elastic strain may best be understood by examination of Figure 13. This figure shows the equivalent strains imposed on a hysteresis loop of a node that has undergone compressive yielding followed by tensile yielding. It should be noted that all equivalent strains are positive scalar values and are referenced from either the initial or a transformed origin. Point "A" is a location on the hysteresis loop where the ϵ_{et} reaches a peak value and unloading begins. This point becomes the new strain reference point from which ϵ_{et}^{**} needs to be calculated. Before this node can load in tension it must elastically

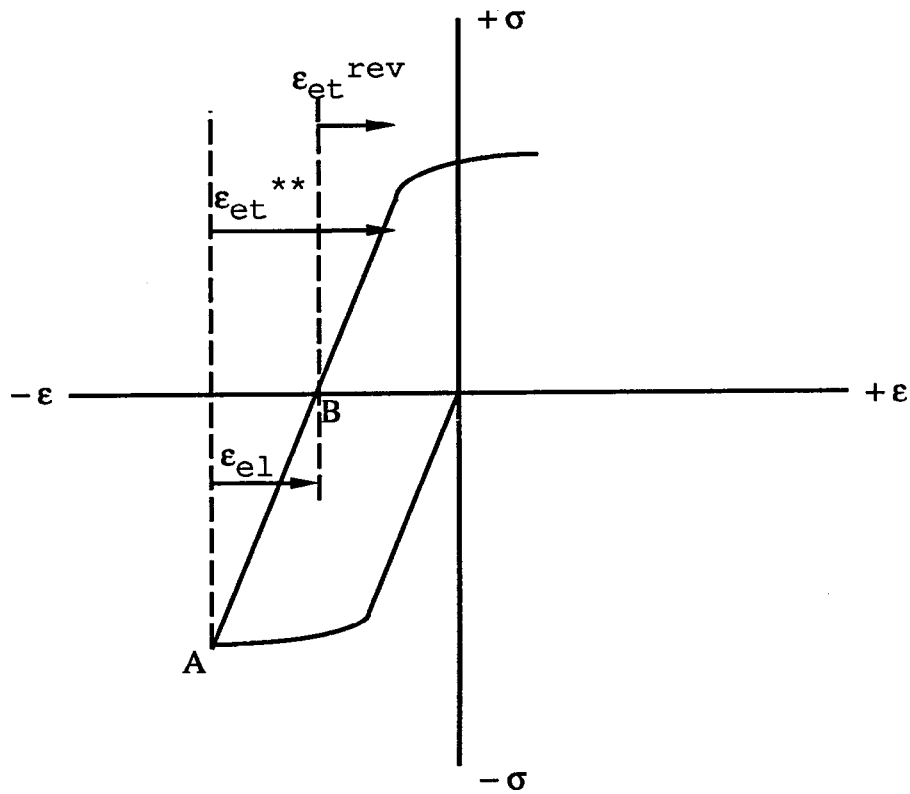


Figure 13. Hysteresis loop of an engineering alloy that has undergone compressive yielding followed by tensile yielding.

unload to point "B". This requires an adjustment in the equivalent total strain as calculated from point "A." The value of equivalent total strain as calculated from point "A" must be decreased by an equivalent elastic strain, ϵ_{el} . The equivalent elastic strain is obtained from the rearrangement of equation [84] and is given as:

$$\epsilon_{el} = \frac{\epsilon_{et}^{pk} - \epsilon_{ep}}{2(1 + \mu)} \quad [105]$$

Mathematically, the adjusted equivalent total strain is expressed as:

$$\epsilon_{et}^{rev} = \epsilon_{et}^{**} - \epsilon_{el} \quad [106]$$

and is called equivalent total reversal strain, ϵ_{et}^{rev} , which is used to determine if yielding occurs for a node that has undergone a stress reversal. Applying this criteria to the plastic component equations and rewriting, one has:

$$\epsilon_{rp}^{**} = \frac{1}{3} \frac{\epsilon_{ep}}{\epsilon_{et}^{rev}} \left[2\epsilon_r^{**} - \epsilon_{\theta}^{**} - \epsilon_z^{**} \right] \quad [107]$$

$$\epsilon_{\theta p}^{**} = \frac{1}{3} \frac{\epsilon_{ep}}{\epsilon_{et}^{rev}} \left[2\epsilon_{\theta}^{**} - \epsilon_r^{**} - \epsilon_z^{**} \right] \quad [108]$$

$$\epsilon_{zp}^{**} = \frac{1}{3} \frac{\epsilon_{ep}}{\epsilon_{et}^{rev}} \left[2\epsilon_z^{**} - \epsilon_r^{**} - \epsilon_{\theta}^{**} \right] \quad [109]$$

where ϵ_{rp}^{**} , $\epsilon_{\theta p}^{**}$, and ϵ_{zp}^{**} are the components of plastic strain for nodes that deformed during the heating phase of the cycle and may deform during the cooling phase of the cycle, and ϵ_r^{**} , ϵ_{θ}^{**} , and ϵ_z^{**} are the transformed strains given by equation [101], [102], and [103], respectively.

Recall from the derivation of the strain equations that the modulus of elasticity, E , and the thermal expansion coefficient, α , were assumed to be constant for the alloy and temperature range under investigation. For a steel-copper-steel composite the values of E and α may vary as much as 80% between the two materials and cannot be used as constants. Introducing E and α into the differential equation as a function of the radius results in a second order nonlinear differential equation with variable coefficients. The solution of the differential equation with variable coefficients would require much greater mathematical rigor than for the case where E and α are constants. A simpler approximate method of treating E and α as a function of the radius would be to substitute the appropriate value of α into the integrals appearing in the strain equations during their evaluation. This requires integrals containing α evaluated from "a to b" to be evaluated as shown in equation [110]:

$$\int_a^b \alpha T r \, dr = \int_a^{Tk1} \alpha_{\text{Steel}} T r \, dr + \int_{Tk1}^{Tk2} \alpha_{\text{Cu}} T r \, dr + \int_{Tk2}^b \alpha_{\text{Steel}} T r \, dr \quad [110]$$

Integrals containing plastic strains are evaluated using the appropriate values of ϵ_{rp} or $\epsilon_{\theta p}$ of steel or copper. Integrals evaluated from "a to r" require a treatment similar to that given by equation [110] but the upper limit of evaluation becomes the r_i node. Similarly, it is required that the appropriate values of E and α be substituted into the stress equations [51], [52], and [53] during calculations.

Incorporation of these equations and techniques into the numerical model is best illustrated by a step-by-step description of the stress analysis logic flow and method of calculation as given in Table 2. The accuracy of this approximation technique is addressed in the Discussion of Results section of this dissertation.

Table 2
Stress Analysis Logic Flow

Step Number	Description of Procedure
	This routine is entered after calculating the temperature profile for the current time step from the thermal section of the numeric model.
1.	Initialize the accumulated plastic strains ϵ_{rp} , $\epsilon_{\theta p}$, and ϵ_{zp} to zero for the first cycle.
2.	Initialize incremental plastic strains $\Delta\epsilon_{rp}$, $\Delta\epsilon_{\theta p}$, and $\Delta\epsilon_{zp}$ to zero at the beginning of each load increment.
3a.	Calculate the value of ϵ_z , C_1 , and C_2 from equations [91], [92], and [93], respectively, making appropriate substitutions for α as shown in equation [110] and using the temperature profile calculated by the thermal part of the model. All integrals are evaluated using the trapezoid rule.
3b.	Compare the values of C_1 and C_2 with those for the previous iteration. If the values agree to six places the solution has converged; go to step 10.
4.	Calculate values for ϵ_{θ} and ϵ_r for each node using equations [89] and [90], respectively. Note: On the zeroth iteration all plastic components are equal to zero and elastic stresses may be calculated from equations [51], [52], and [53] and used for comparison with elastic-plastic stress calculations after convergence occurs.
5.	Using equation [97] calculate an equivalent total strain for each node, from the values of ϵ_r , ϵ_{θ} , and ϵ_z obtained in step 4.
6.	Calculate an equivalent plastic strain for each node, using the equation that represents the node's thermo-mechanical properties as shown in Figures 16 and 17. If the calculated value for ϵ_{ep} is negative set it equal to zero.
7.	Calculate the plastic components of strain from equations [98], [99], and [100] for the values obtained in steps 4, 5, and 6.
8.	Substitute the plastic components values ϵ_{rp} and $\epsilon_{\theta p}$ into $\Delta\epsilon_{rp}$ and $\Delta\epsilon_{\theta p}$, respectively.
9.	Go to step 3a where the solution will be altered due to the introduction of plastic strain values into the integrals.

Table 2 (Continued)

10. Convergence has occurred. Compare equivalent total strain value with that of the previous time increment to determine if the peak value of ϵ_{et} has been reached for any node. If so, save values of ϵ_{θ} , ϵ_r , and ϵ_z for new reference point.
11. Sum plastic strains of this load increment with prior load increments using equations (a, b, c, and d):
 - (a) $\Sigma\Delta\epsilon_{rp} = \Sigma\Delta\epsilon'_{rp} + \Delta\epsilon_{rp}$
 - (b) $\Sigma\Delta\epsilon_{\theta p} = \Sigma\Delta\epsilon'_{\theta p} + \Delta\epsilon_{\theta p}$
 - (c) $\Sigma\Delta\epsilon_{zp} = \Sigma\Delta\epsilon'_{zp} + \Delta\epsilon_{zp}$
 - (d) $\Sigma\Delta\epsilon_{ep} = \Sigma\Delta\epsilon'_{ep} + \Delta\epsilon_{ep}$
 where the prime indicates prior load increments.
12. Calculate σ_r , σ_{θ} , and σ_z from equations [51], [52], and [53], respectively.
13. Check for completion of thermal cycle. If complete go to step 14; if not return to thermal model (Table 1, step 5).
14. Compare strain values of previous cycle with strain values of the current cycle to determine if cyclic equilibrium has been obtained. If values agree within desired criteria the solution is complete; go to step 15. If values do not agree, calculate additional cycles by going to thermal model (Table 1, step 5).
15. Print results.

IV. OPTIMIZATION OF A MULTILAYERED CYLINDRICAL SHELL WITH THE THERMO-ELASTIC-PLASTIC NUMERICAL MODEL

The thermo-elastic-plastic numerical model developed in the previous sections of this dissertation was used in this section to analyze and optimize the thermal fatigue life of a multilayered cylindrical shell. To restrict the number of cases to be analyzed several constraints were placed on the cylinder's design. Depending on the manufacturing process, it is conceivable that many unique residual stress patterns could exist in composite tubing. Although the numerical model could be used to determine the effect of residual stresses on the thermal fatigue life of a composite design, for demonstration purposes the residual stresses are assumed to be zero. This assumption provides a consistent starting point from which tube designs may be evaluated. Other constraints include a high strength 2 1/4% Chromium-1.0% Molybdenum steel for the ID and OD layers and Oxygen Free, High Conductivity (OFHC) copper for the middle layer. A heat source temperature of 900 C and heat transfer coefficients of 4700 Watts/m² and 1575 Watts/m² were used for the ID and OD, respectively. A cycle time of 35 seconds (10 seconds heating and 25 seconds cooling) was selected to give a thermal gradient sufficient to cause plastic strains in the tube. The ID was fixed at 50 cm and the ID and OD layer thicknesses

were constrained to a minimum value of 3 mm. The layer thicknesses were varied in 3 mm increments in each of the test designs. The total thickness was required to be 3 cm. These constraints are summarized in Tables 3 and 4, which give thermophysical properties for the steel and copper (Table 3) and physical dimensions, mechanical properties, and thermal constraints imposed on the design (Table 4). Figures 14 and 15 show the stress-strain curves, obtained from a commercial testing laboratory, for the steel and copper, respectively, and Figures 16 and 17 are the equivalent plastic strain and equivalent total strain relationships regressed from these stress-strain curves.

After incorporation of these data into the numerical model, the numerical program written in Fortran 77 was run on a desk top computer (Apple Macintosh II). The results available from the model include the temperature; the radial, tangential, and axial stresses; the radial, tangential, and axial strains; the radial displacement; and the plastic strains, all as a function of radius and time.

Typical results from the model for a tube with a 25 cm radius, 6 mm ID layer of steel, 18 mm middle layer of copper, and 6 mm OD layer of steel are presented in graphic form in Figures 18 through 32 for the first thermal cycle. Figure 18 shows the temperature profile in the tube one second after heat was applied to the ID. The low thermal diffusivity of the steel results in a steep thermal gradient. Figures 19, 20, and 21 show the radial, tangential, and axial stress

Table 3
Thermophysical Properties

The thermophysical properties of the steel were:

1. Thermal conductivity:

$$k_{\text{Steel}} = 9.575 - 6.591 \times 10^{-4} T - 1.205 \times 10^{-6} T^2 \quad \frac{\text{cal}}{\text{sec m C}}$$

2. Density:

$$\rho_{\text{Steel}} = 7.86 - 0.168 \times 10^{-4} T \quad \frac{\text{g}}{\text{cm}^3}$$

3. Specific heat:

$$C_{p\text{Steel}} = 0.11 + 5.62 \times 10^{-5} T \quad \frac{\text{cal}}{\text{g C}}$$

4 Thermal expansion coefficient:

$$\alpha_{\text{Steel}} = 3.711 \times 10^{-6} + 3.81 \times 10^{-10} T \quad \text{C}^{-1}$$

The thermophysical properties of the copper were:

1. Thermal conductivity:

$$k_{\text{Copper}} = 90.01 - 5.726 \times 10^{-3} T - 7.843 \times 10^{-6} T^2 \quad \frac{\text{cal}}{\text{sec m C}}$$

2. Density:

$$\rho_{\text{Copper}} = 8.94 - 3.23 \times 10^{-5} T \quad \frac{\text{g}}{\text{cm}^3}$$

3. Specific heat:

$$C_{p\text{Copper}} = 0.0924 + 12.6 \times 10^{-6} T \quad \frac{\text{cal}}{\text{g C}}$$

4 Thermal expansion coefficient:

$$\alpha_{\text{Copper}} = 4.780 \times 10^{-6} + 1.0 \times 10^{-9} T \quad \text{C}^{-1}$$

Table 4
Physical Dimensions, Mechanical Properties, and Thermal
Loading Constraints

The physical dimensions and mechanical properties were:

1. Inside diameter of the tube was 50.00 cm.
2. The total wall thickness was 3.00 cm.
3. Modulus of Elasticity of steel:

$$E_{\text{Steel}} = 2.152 \times 10^5 - 18.29 T - 2.364 \times 10^{-2} T^2 \text{ MPa}$$
4. Modulus of Elasticity of copper:

$$E_{\text{Copper}} = 1.277 \times 10^5 - 14.07 T - 1.458 \times 10^{-2} T^2 \text{ MPa}$$
5. Stress-strain data for the steel and copper are shown in Figures 14 and 15. Equivalent total and equivalent plastic strain data taken from these stress strain curves are given in Figures 16 and 17.

The thermal constraints were:

6. Initial composite temperature was 25 C.
7. Flame temperature was 900 C.
8. Cooling water temperature was 25 C.
9. ID heat transfer coefficient was 4700 Watts/m².
10. OD heat transfer coefficient was 1575 Watts/m² if the OD temperature was less than 100 C and was 3150 Watts/m² if greater than or equal to 100 C.
11. Heating phase of cycle was 10.00 seconds.
12. Cooling phase of cycle was 25.00 seconds.
13. Total cycle time of 35.00 seconds.

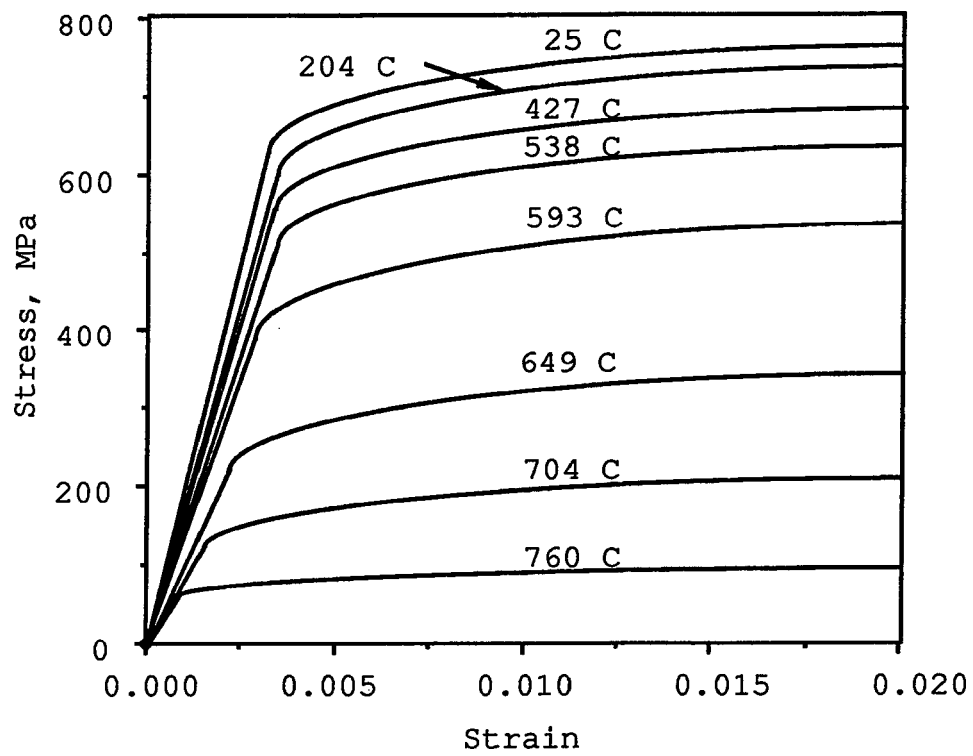


Figure 14. Stress-strain curves at selected temperatures for 2 1/4% Cr-1% Mo steel.

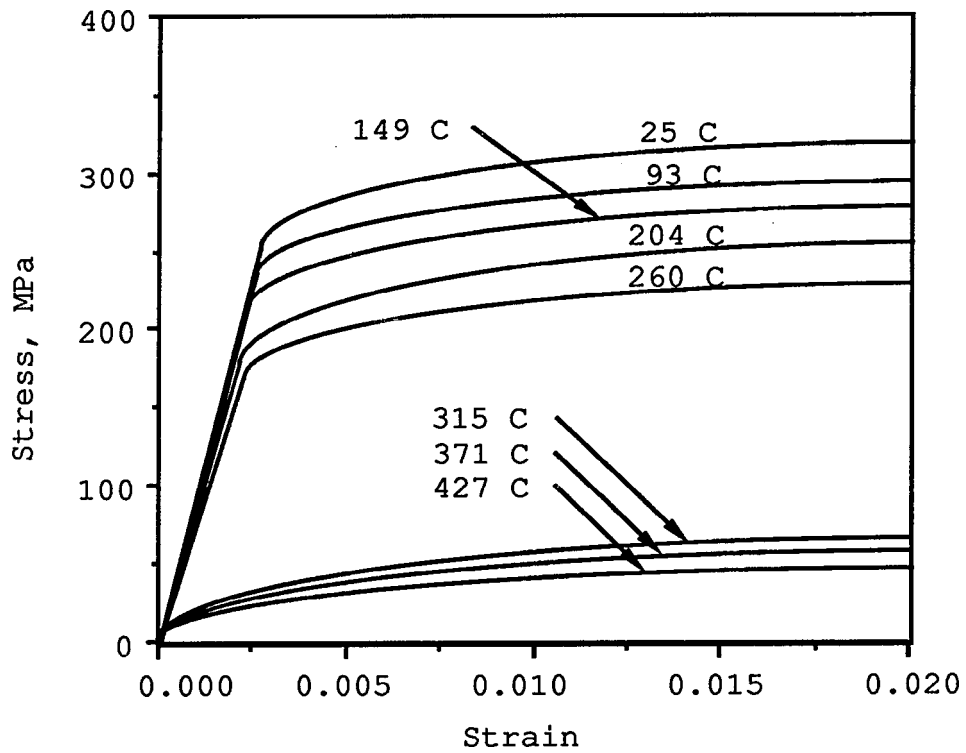


Figure 15. Stress-strain curves of OFHC copper at selected temperatures.

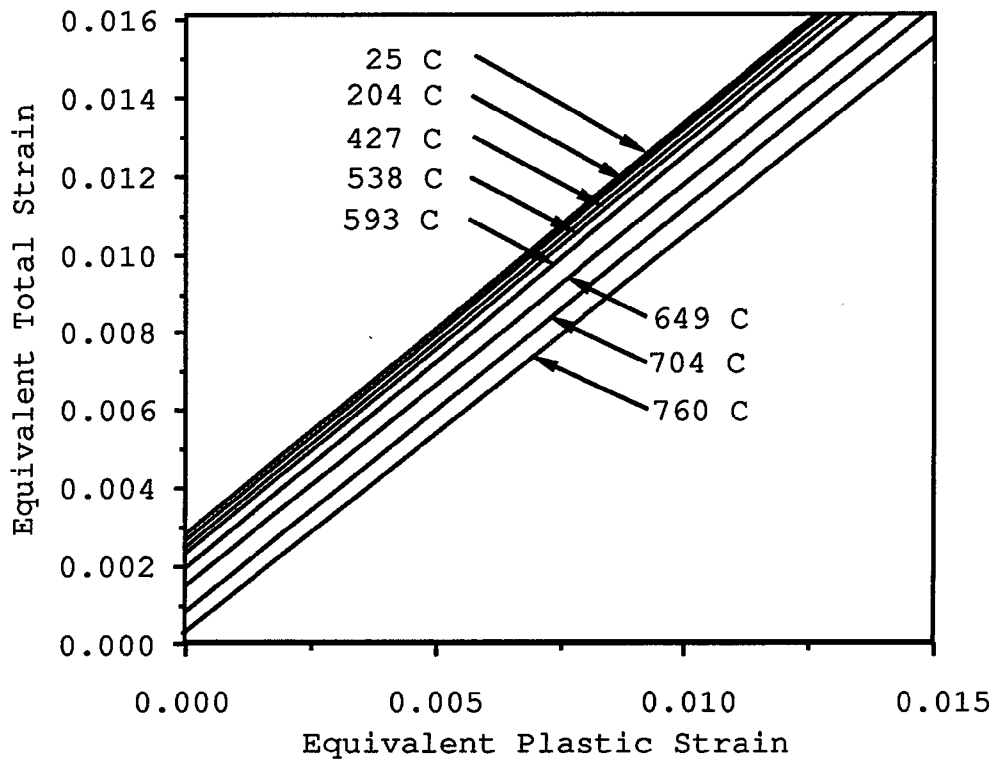


Figure 16. Equivalent total and equivalent plastic strain relationship for 2 1/4% Cr-1% Mo steel at selected temperatures.

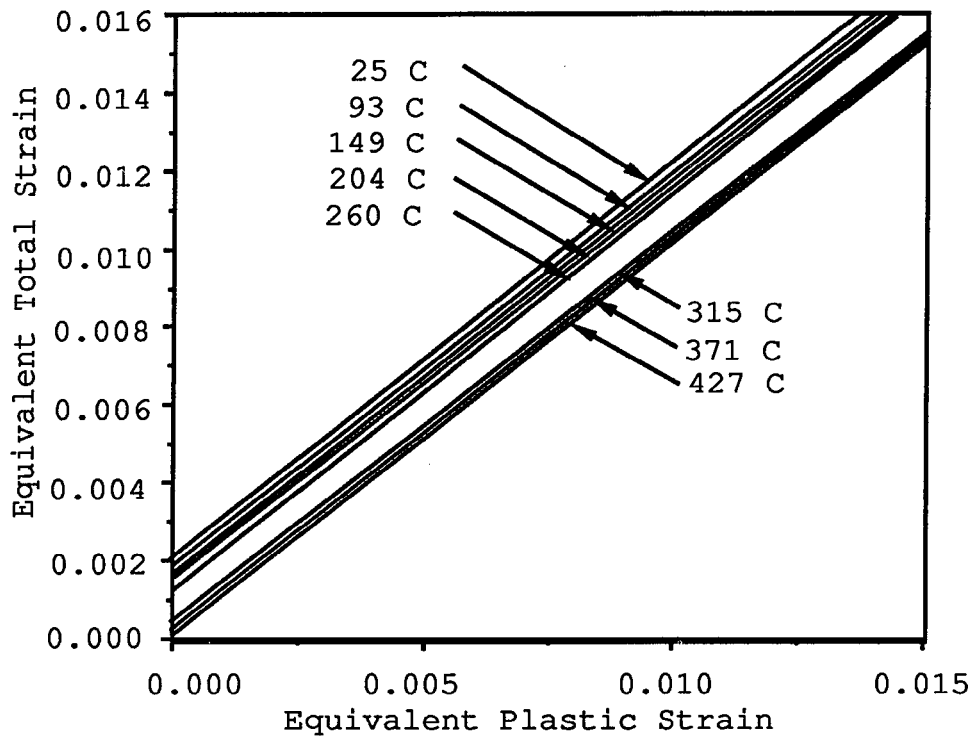


Figure 17. Equivalent total and equivalent plastic strain relationship for OFHC copper at selected temperatures.

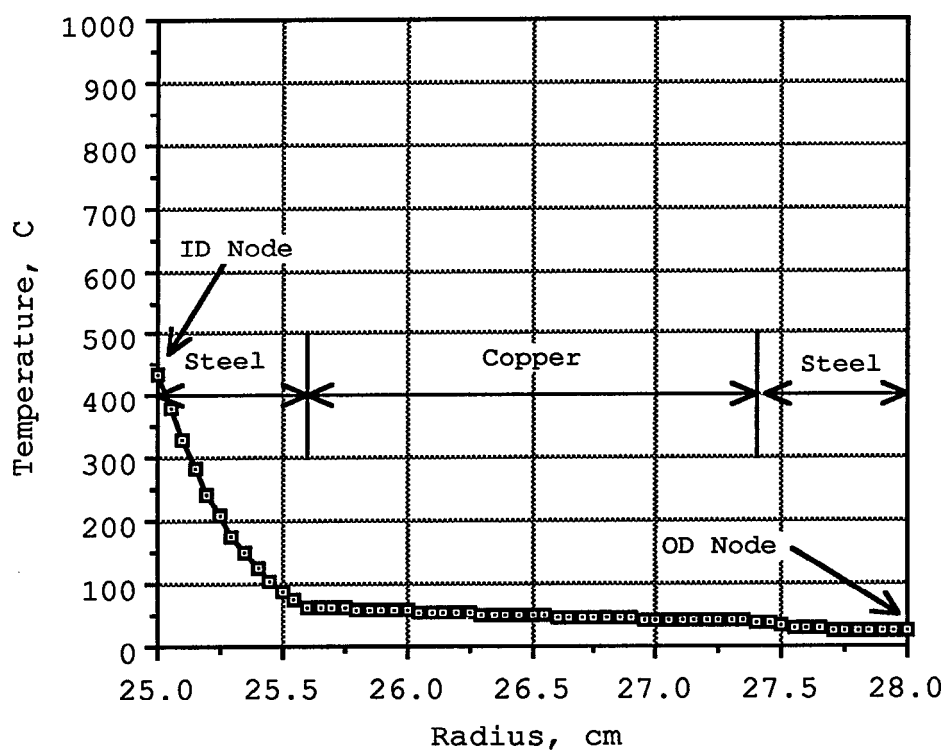


Figure 18. Radial temperature profile in a composite tube with a 6 mm steel ID layer-18 mm copper middle layer-6 mm steel OD layer 1 second into the heating phase of a thermal cycle.

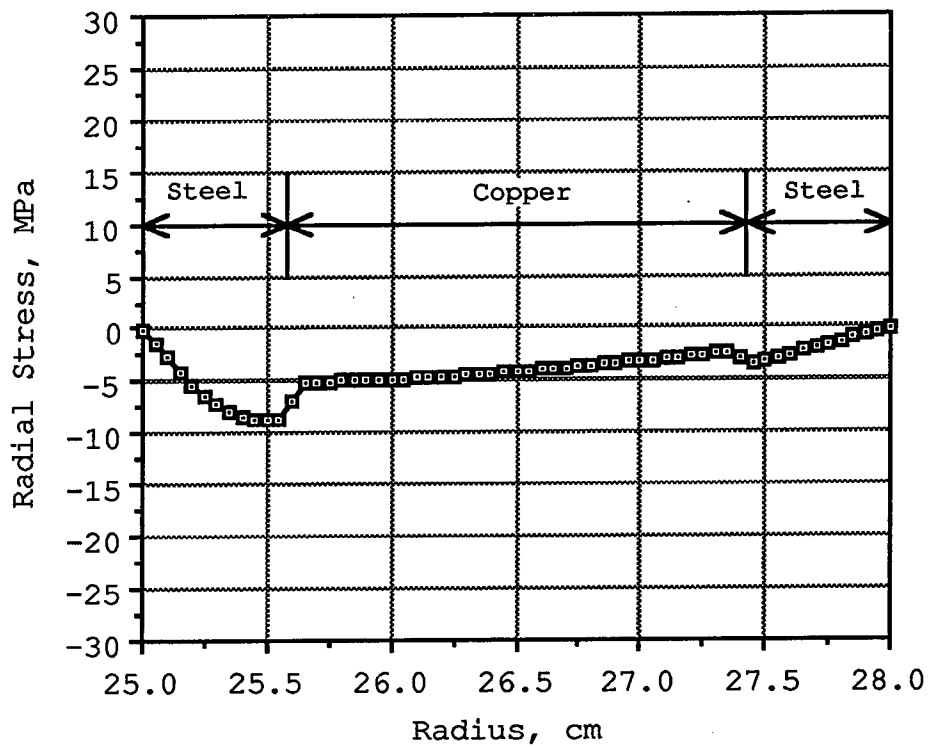


Figure 19. Radial stress profile in a composite tube with a 6 mm steel ID layer-18 mm copper middle layer-6 mm steel OD layer 1 second into the heating phase of a thermal cycle.

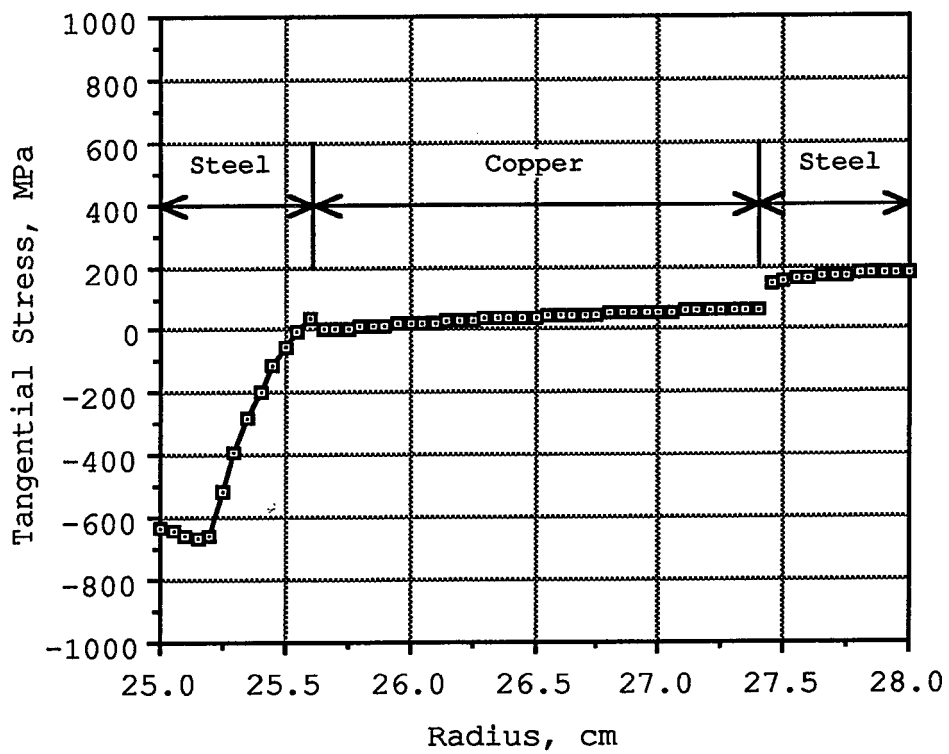


Figure 20. Tangential stress profile in a composite tube with a 6 mm steel ID layer-18 mm copper middle layer-6 mm steel OD layer 1 second into the heating phase of a thermal cycle.

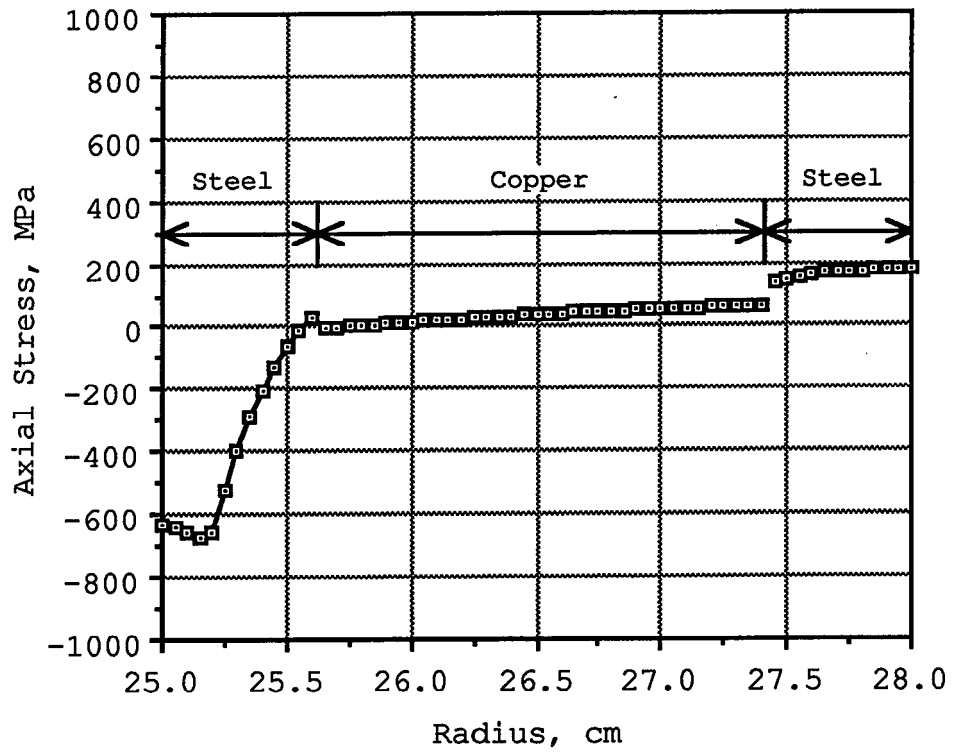


Figure 21. Axial stress profile in a composite tube with a 6 mm steel ID layer-18 mm copper middle layer-6 mm steel OD layer 1 second into the heating phase of a thermal cycle.

profiles induced by the thermal gradient at the end of one second of heating. These stress profiles developed as a result of the cooler outer layers constraining the thermal expansion of the higher temperature inner layer. Figures 22 and 23 show the equivalent stress and equivalent plastic strain profiles, respectively, for one second of heating. It is apparent that the first four nodes in the ID layer yielded as a result of the high equivalent stress and reduced yield strength.

At ten seconds into the thermal cycle, the ID node reached a peak temperature of about 720 C. Again, as shown in Figure 24, both ID and OD steel layers exhibited steep thermal gradients. The copper, with its high thermal diffusivity, effectively transferred heat from the ID to the OD, which raised the mean temperature of the OD steel layer to a value higher than that in a comparable all steel tube. The higher mean temperature of the OD layer resulted in increased thermal expansion and reduced stresses in the OD layer. Figures 25 through 27 show the radial, tangential, and axial stress profiles at ten seconds into the thermal cycle. It is apparent from the equivalent stress and equivalent plastic strain profiles shown in Figures 28 and 29, respectively, that yielding has occurred for several nodes in the ID and OD layers of this design. Due to the yielding in both ID and OD layers, it is likely that this design would be geometrically unstable and go "out of round" during thermal cycling.

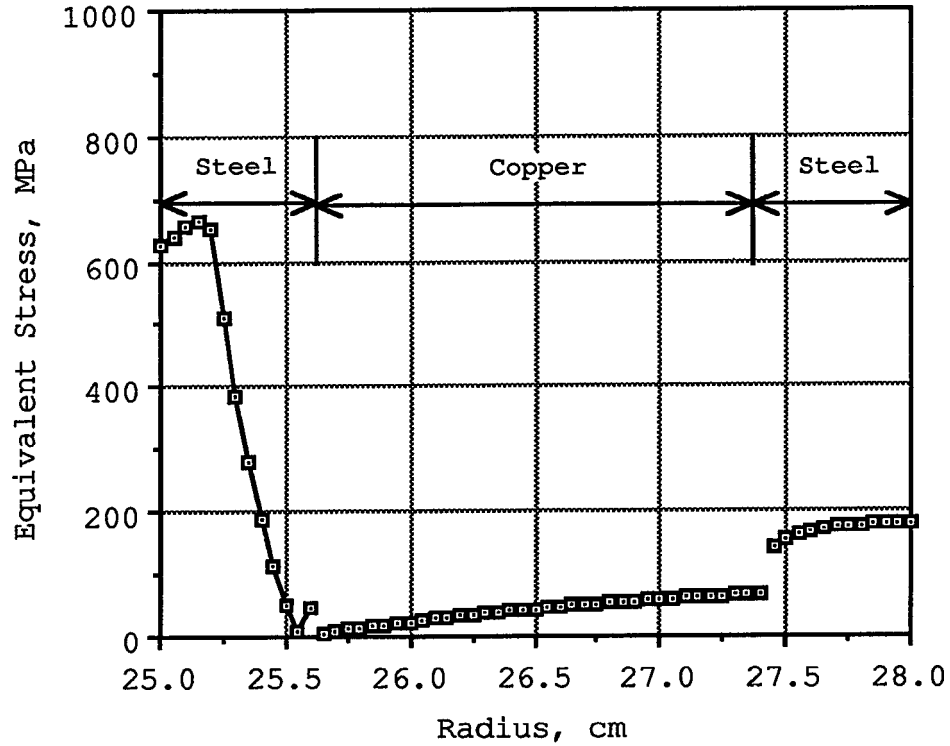


Figure 22. Equivalent stress profile in a composite tube with a 6 mm steel ID layer-18 mm copper middle layer-6 mm steel OD layer 1 second into the heating phase of a thermal cycle.

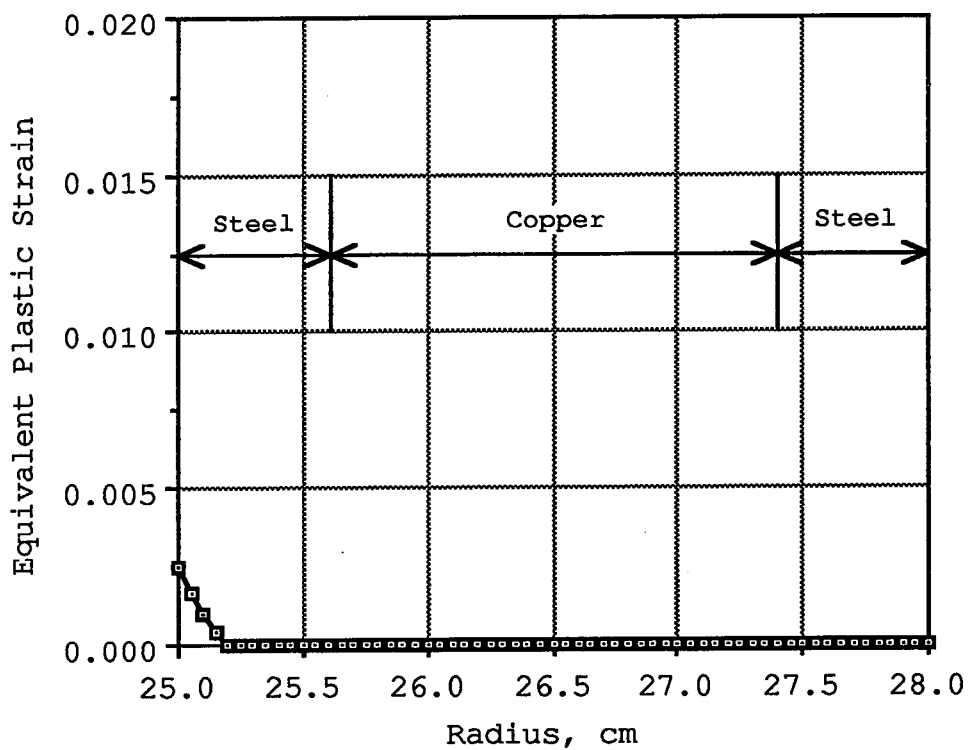


Figure 23. Equivalent plastic strain profile in a composite tube with a 6 mm steel ID layer-18 mm copper middle layer-6 mm steel OD layer 1 second into the heating phase of a thermal cycle.

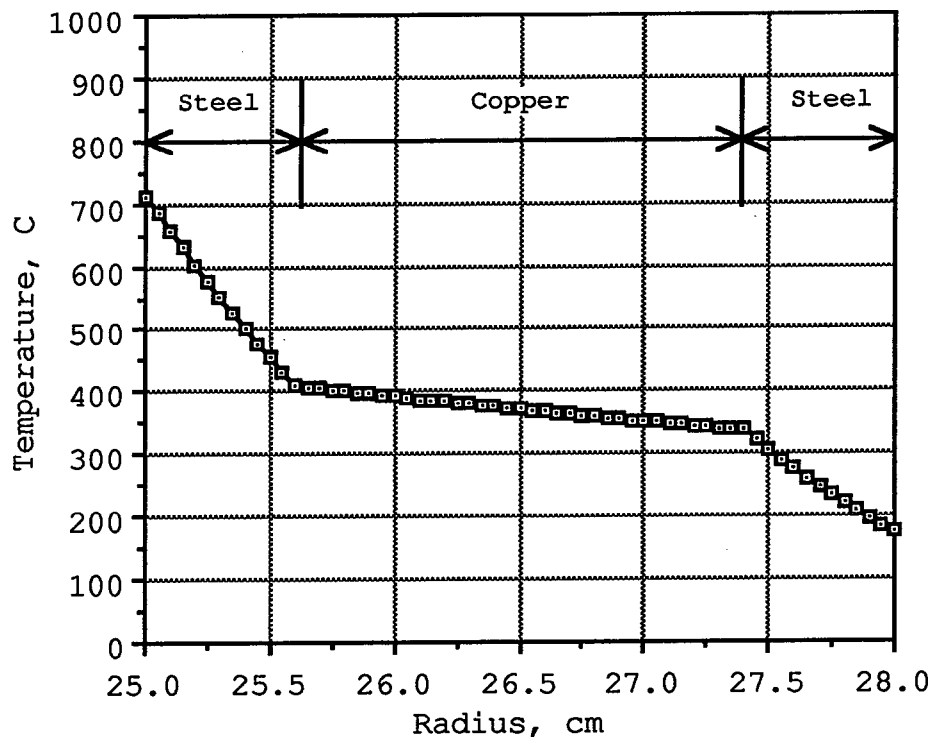


Figure 24. Radial temperature profile in a composite tube with a 6 mm steel ID layer-18 mm copper middle layer-6 mm steel OD layer 10 seconds into the heating phase of a thermal cycle.

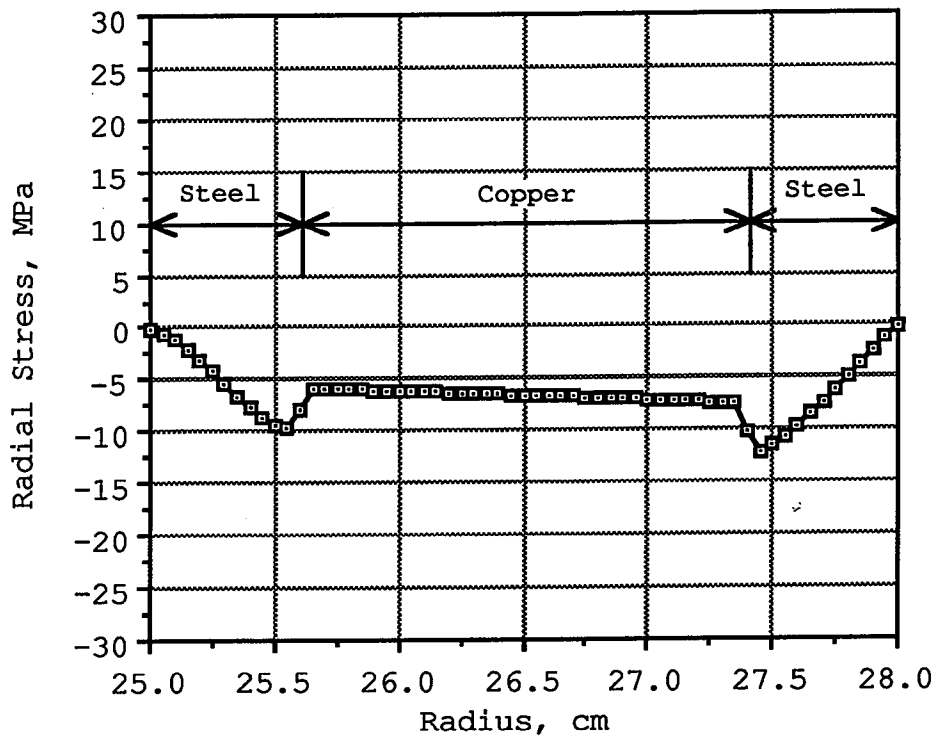


Figure 25. Radial stress profile in a composite tube with a 6 mm steel ID layer-18 mm copper middle layer-6 mm steel OD layer 10 seconds into heating phase of a thermal cycle.

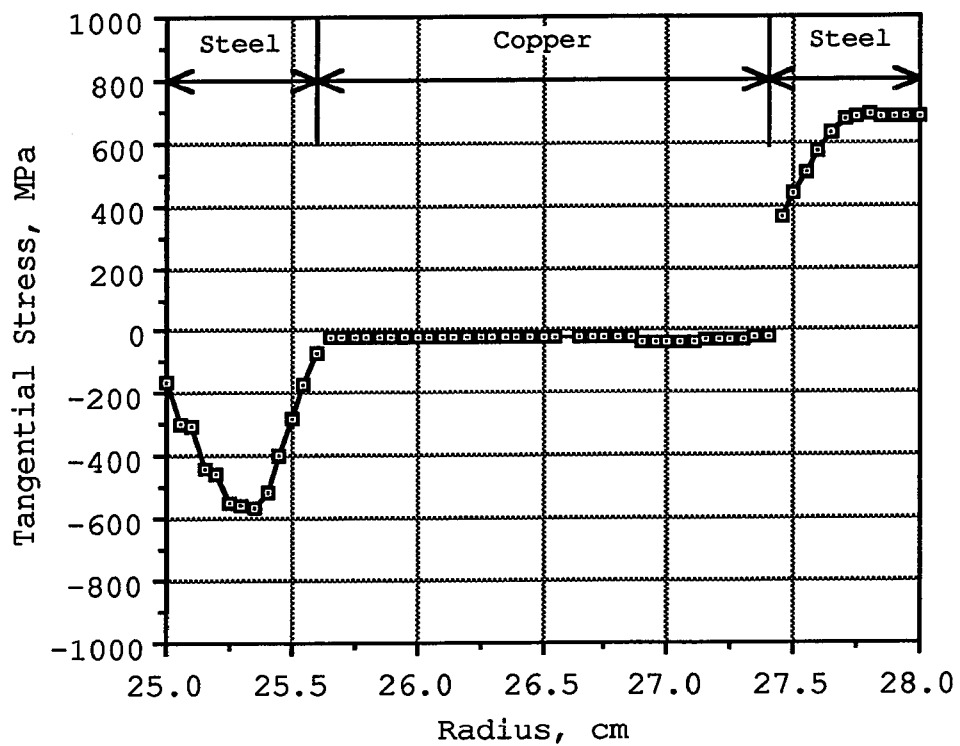


Figure 26. Tangential stress profile in a composite tube with a 6 mm steel ID layer-18 mm copper middle layer-6 mm steel OD layer 10 seconds into the heating phase of a thermal cycle.

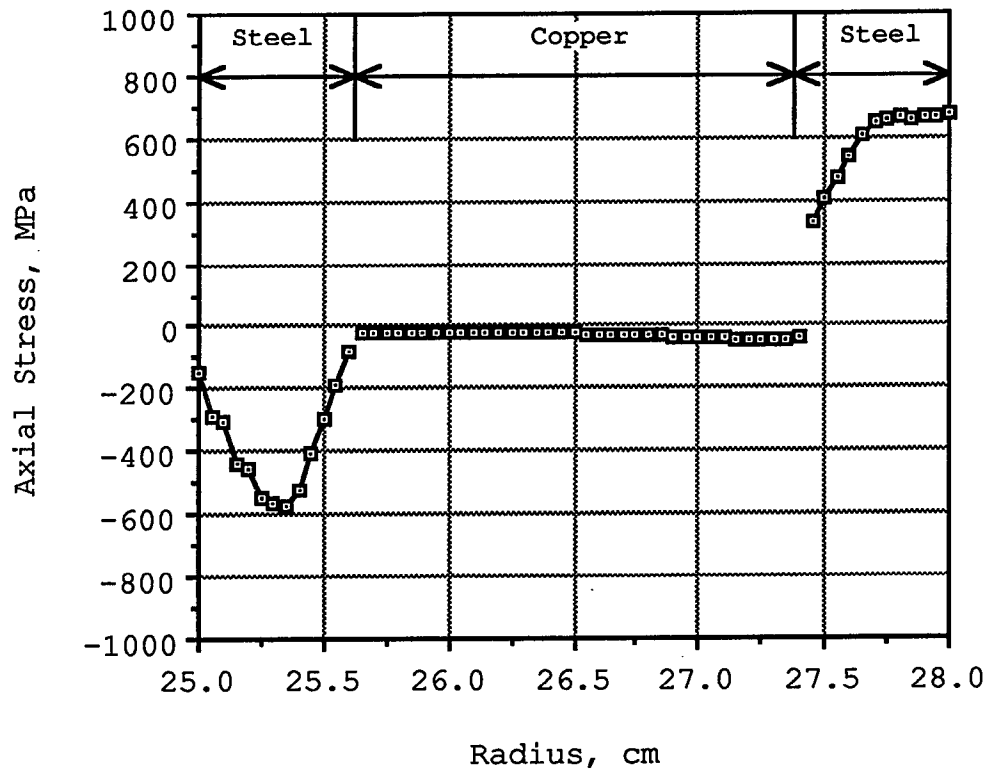


Figure 27. Axial stress profile in a composite tube with a 6 mm steel ID layer-18 mm copper middle layer-6 mm steel OD layer 10 seconds into the heating phase of a thermal cycle.

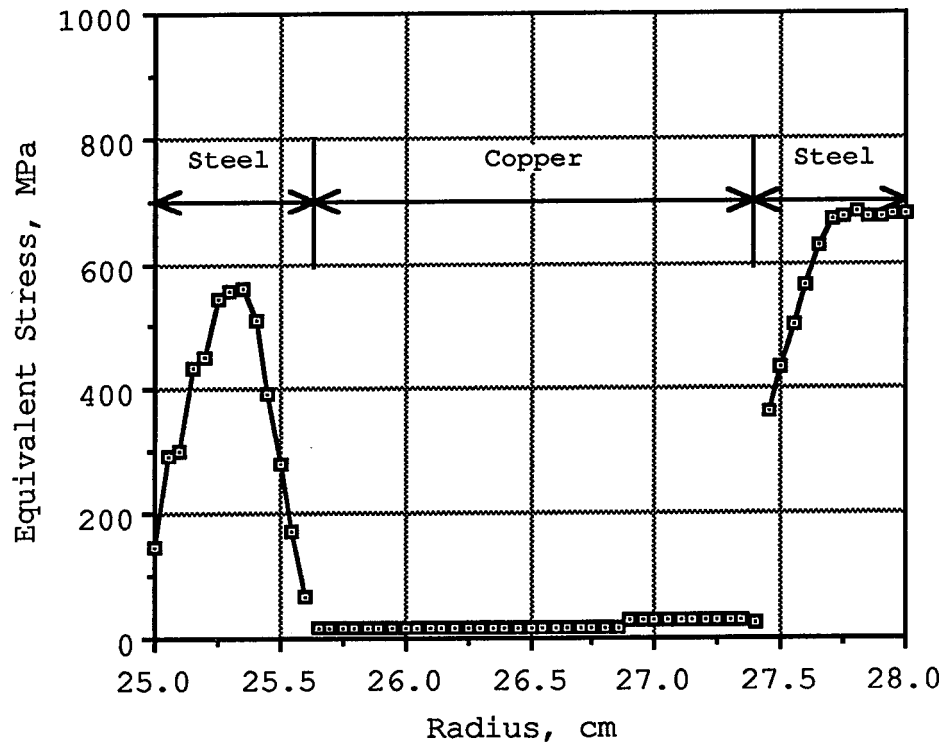


Figure 28. Equivalent stress profile in a composite tube with a 6 mm steel ID layer-18 mm copper middle layer-6 mm steel OD layer 10 seconds into the heating phase of a thermal cycle.

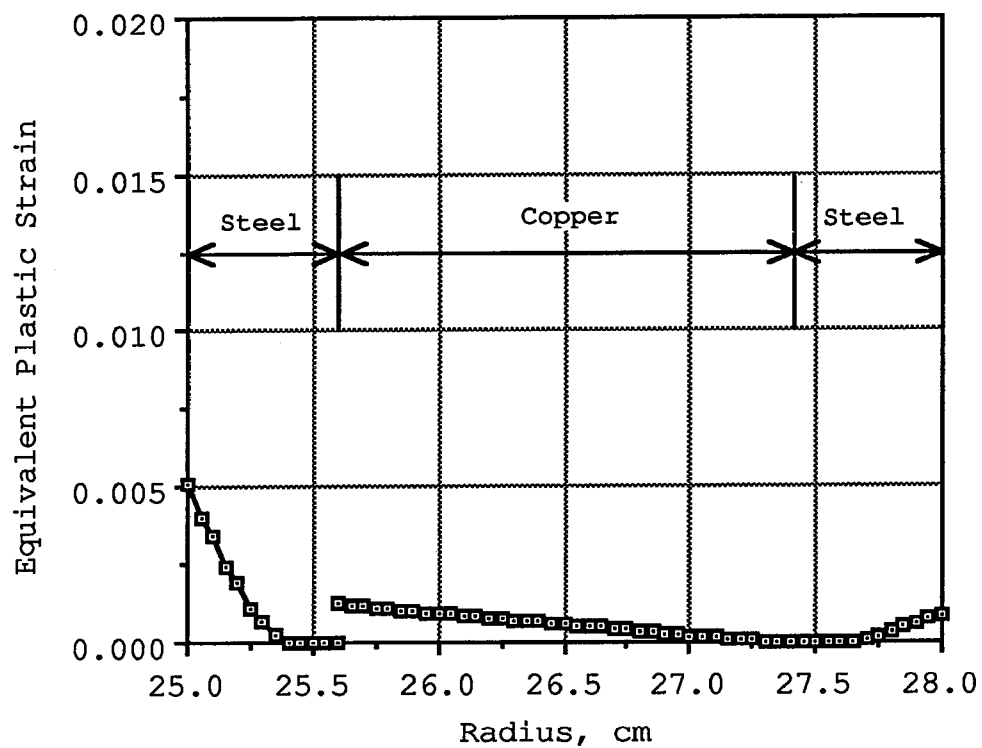


Figure 29. Equivalent plastic strain profile in a composite tube with a 6 mm steel ID layer-18 mm copper middle layer-6 mm steel OD layer 10 seconds into the heating phase of a thermal cycle.

At the 35th second of a thermal cycle (25 seconds into the cooling phase) the thermal gradient, as shown in Figure 30, was low and fairly close to the initial temperature of 25 C. The radial, tangential, axial, and equivalent stresses, at this point in the thermal cycle, are shown in Figures 31 through 34, respectively. These stresses were present at the end of the first thermal cycle and may be thought of as the residual stresses at the beginning of the second thermal cycle. It should be noted from the equivalent plastic strain profile as shown in Figure 35 that some nodes which yielded during the heating phase also yielded in an opposite sense during the cooling phase. Nodes that yielded and strain hardened during the first thermal cycle may or may not yield during subsequent cycles.

Figure 36 shows the temperature response of the ID surface node for six thermal cycles. Notice that a repetitive thermal cycle is established after five cycles. The total radial and tangential strains, shown in Figure 37, also establish a repetitive pattern after the fifth thermal cycle. Figure 38 shows a detailed graph of the total strains, ϵ_r , ϵ_θ , and ϵ_z , for the first thermal cycle.

It should be evident from the above figures that the numerical model's ability to calculate temperatures, stresses, and strains occurring in cylindrical shells during the heating and cooling phases of a thermal cycle gives the designer great insight into the dynamic nature of thermal stress problems.

To determine the best tube design, within the given constraints, a strain range for each node was calculated from data taken from the fifth thermal cycle. The fifth cycle was

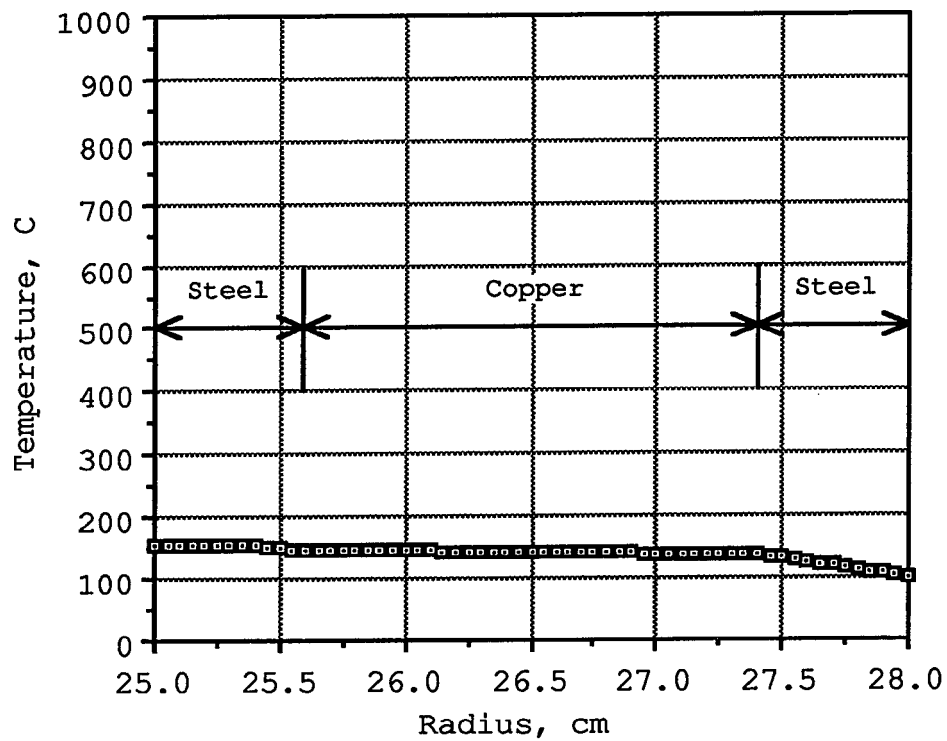


Figure 30. Radial temperature profile in a composite tube with a 6 mm steel ID layer-18 mm copper middle layer-6 mm steel OD layer 35 seconds into a thermal cycle.

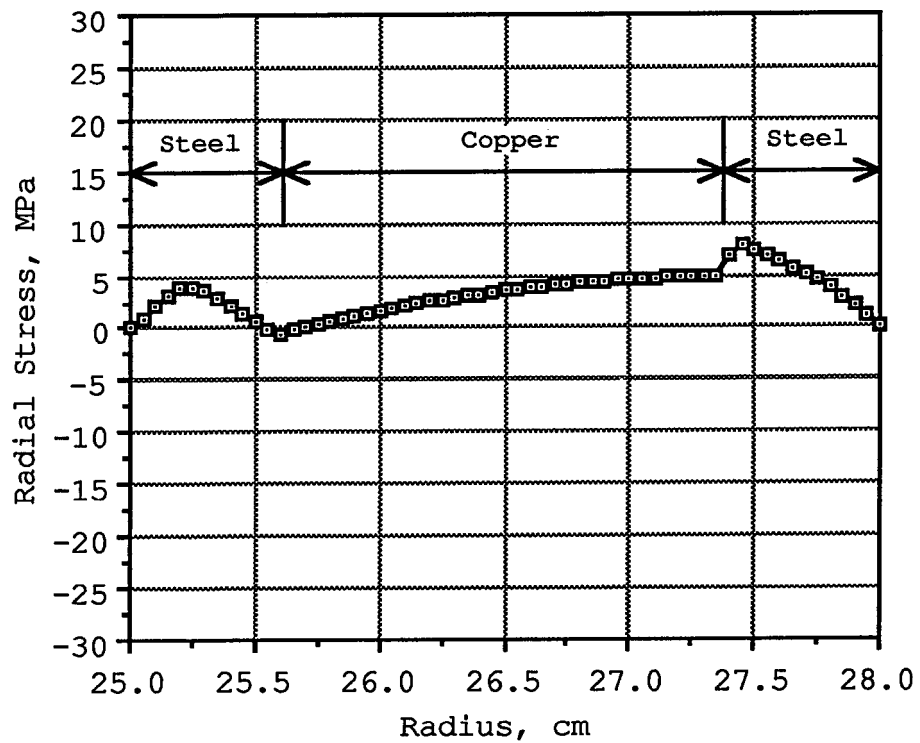


Figure 31. Radial stress profile in a composite tube with a 6 mm steel ID layer-18 mm copper middle layer-6 mm steel OD layer 35 seconds into a thermal cycle.

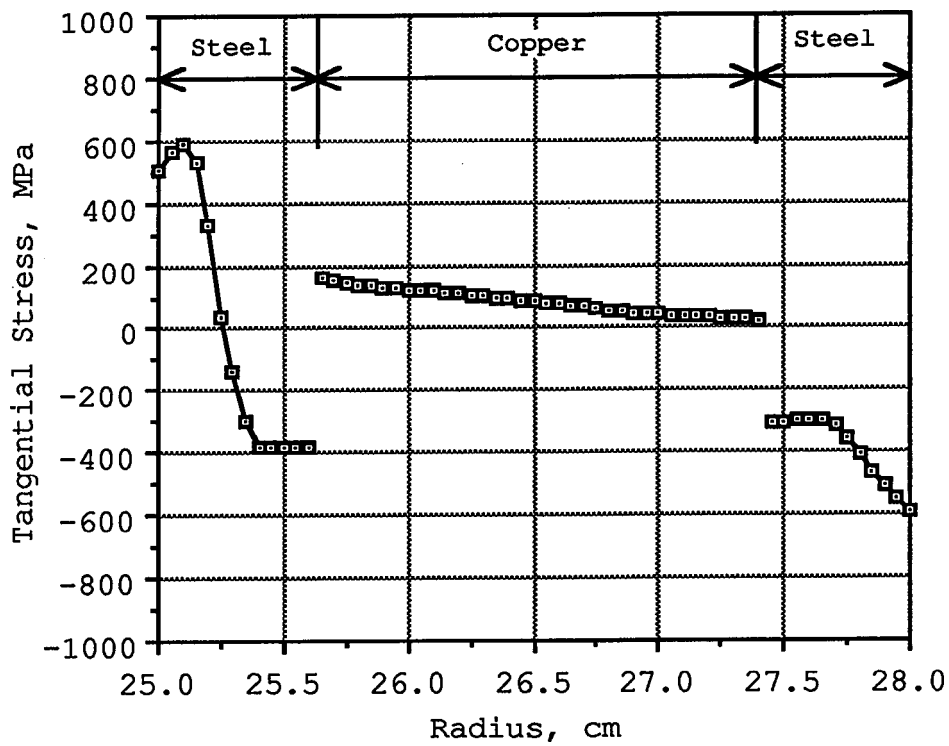


Figure 32. Tangential stress profile in a composite tube with a 6 mm steel ID layer-18 mm copper middle layer-6 mm steel OD layer 35 seconds into a thermal cycle.

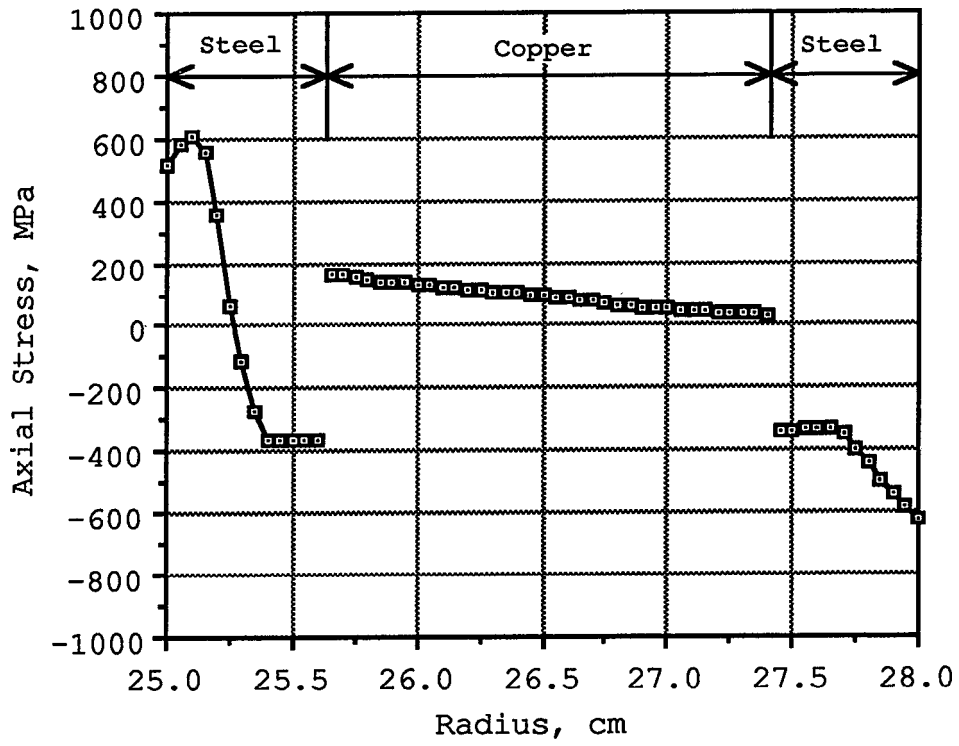


Figure 33. Axial stress profile in a composite tube with a 6 mm steel ID layer-18 mm copper middle layer-6 mm steel OD layer 35 seconds into a thermal cycle.

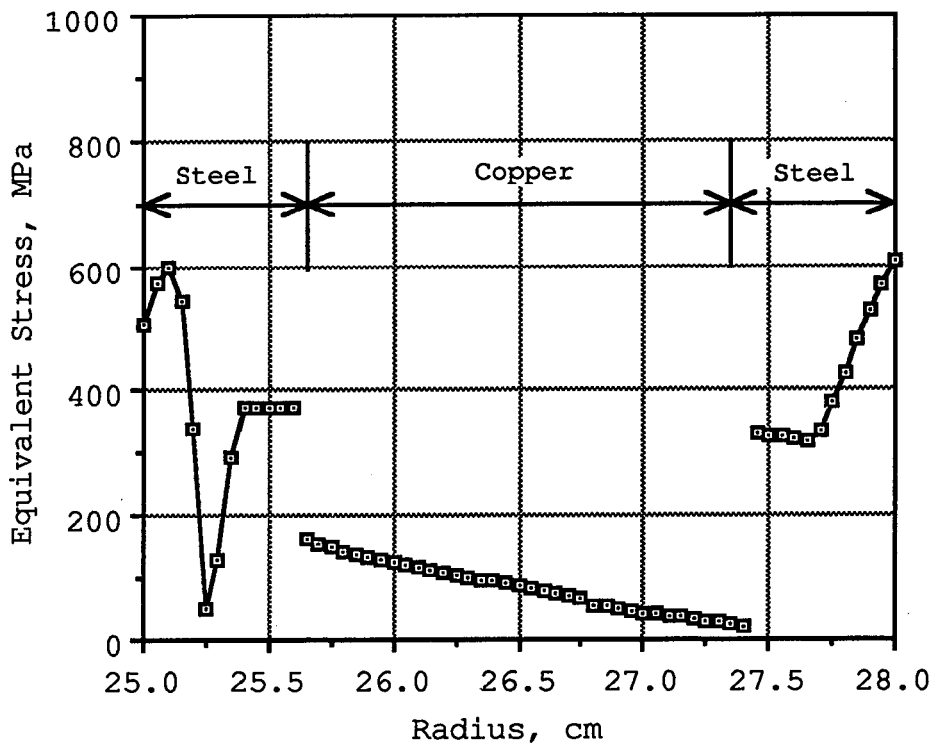


Figure 34. Equivalent stress profile in a composite tube with a 6 mm steel ID layer-18 mm copper middle layer-6 mm steel OD layer 35 seconds into a thermal cycle.

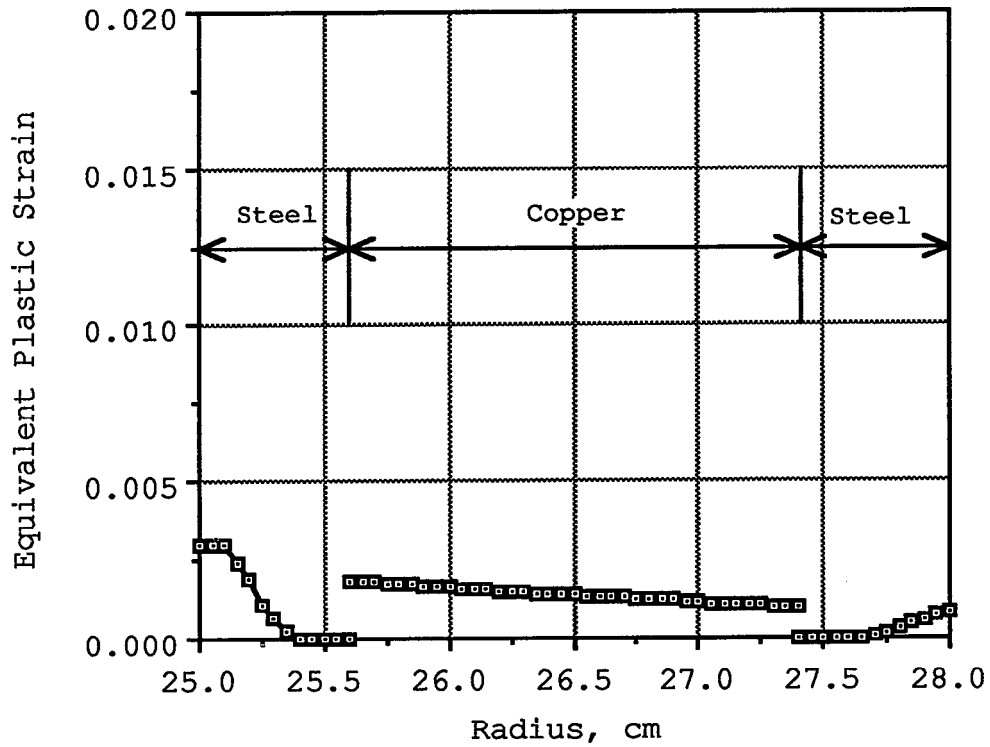


Figure 35. Equivalent plastic strain profile in a composite tube with a 6 mm steel ID layer-18 mm copper middle layer-6 mm steel OD layer 35 seconds into a thermal cycle.

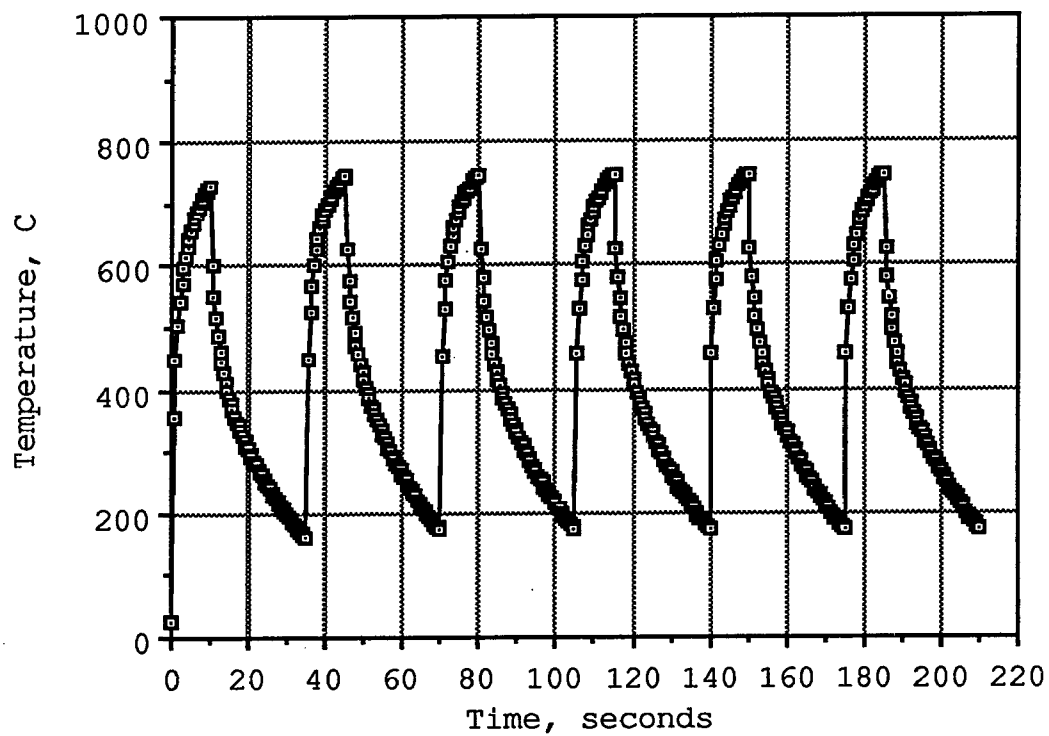


Figure 36. Transient temperature response of the ID node for 6 thermal cycles.

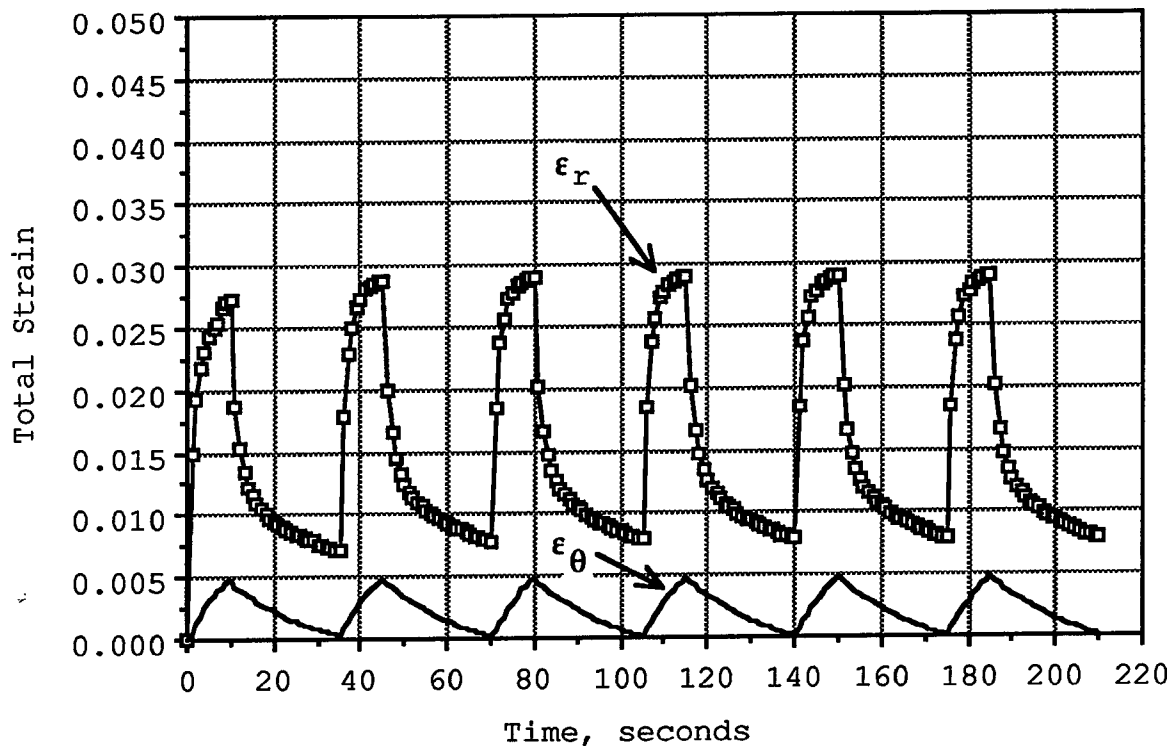


Figure 37. Total radial and tangential strains as a function of thermal cycling.

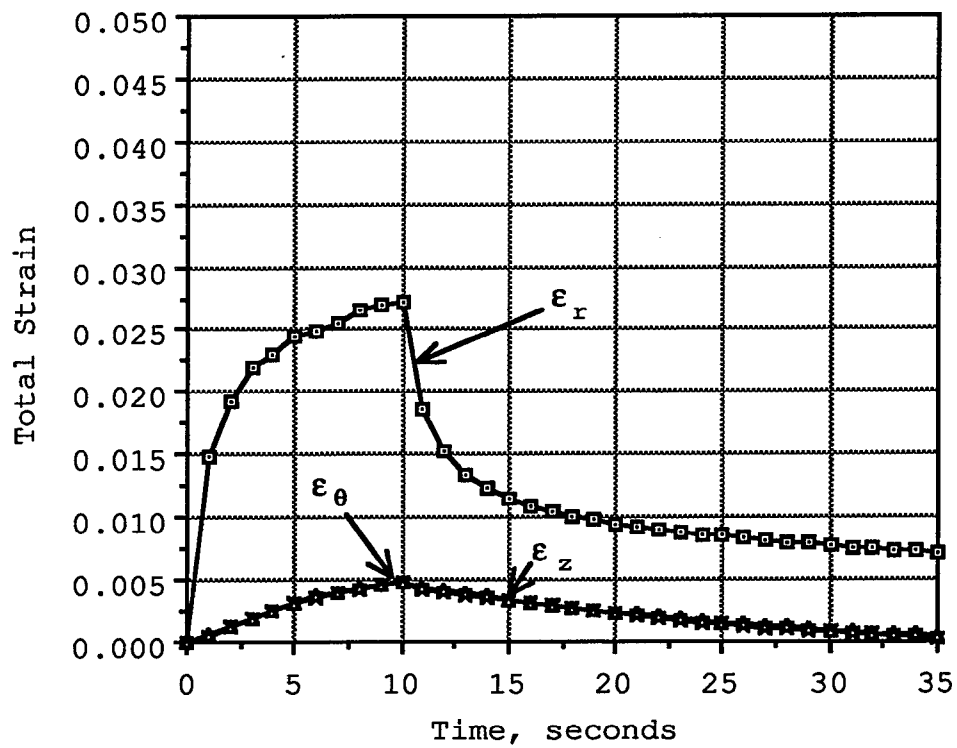


Figure 38. Principal total strains for one thermal cycle.

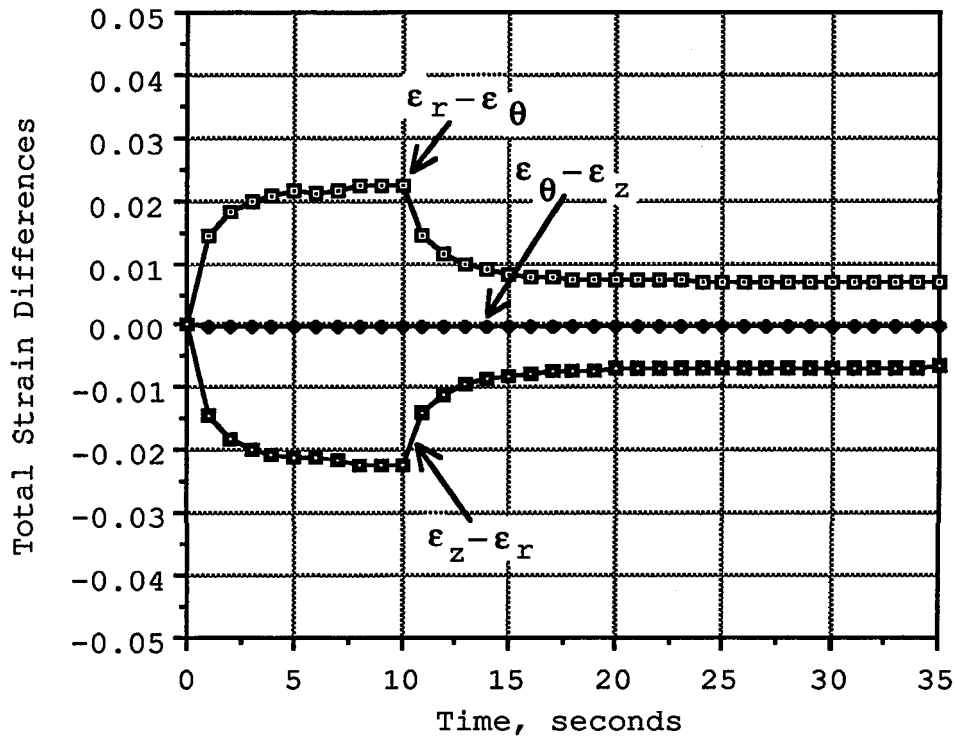
chosen because there was no significant difference between the fifth and subsequent cycles. Strain differences, which were used to calculate a strain range, were scanned from the beginning to the end of the thermal cycle to find the nodes which had the smallest and largest values in each of the three layers. Typical values of the strain differences for the ID node are shown graphically in Figure 39. Once the maximum and minimum values of the strain differences were found, the ranges of these strain differences were calculated by subtracting the minimum from the maximum value. The ranges of the strain differences were substituted into equation [111] and the strain range was calculated.

$$\Delta\varepsilon = \frac{\sqrt{2}}{3} \sqrt{\left[\Delta(\varepsilon_r - \varepsilon_\theta)\right]^2 + \left[\Delta(\varepsilon_r - \varepsilon_z)\right]^2 + \left[\Delta(\varepsilon_\theta - \varepsilon_z)\right]^2} \quad [111]$$

Delta in equation [111] indicates the range of strain differences. These strain range values, along with the strain range vs. cycles to failure graphs shown in Figures 40¹³ and 41,¹⁴ were used to determine the cyclic life of each node. The node with the minimum life within a layer represents the life of the layer and the layer with the minimum life, the life of the design.

To determine the optimum tube design, layer thicknesses were varied in 3 mm increments while holding total thickness, heat input, cycle time, and other variables constant. This resulted in the analysis of 21 different tube designs.

The tube design, range of strain differences, strain range, layer life, and design life values are tabulated in Table 5. The tube design is given in the form of TK1-TK2-TK3,



$$\Delta\epsilon = \frac{\sqrt{2}}{3} \sqrt{\Delta (\epsilon_r - \epsilon_\theta)^2 + \Delta (\epsilon_\theta - \epsilon_z)^2 + \Delta (\epsilon_z - \epsilon_r)^2}$$

$$\Delta\epsilon = 0.0146$$

Figure 39. Total strain differences (for the ID surface node) for a thermal cycle.

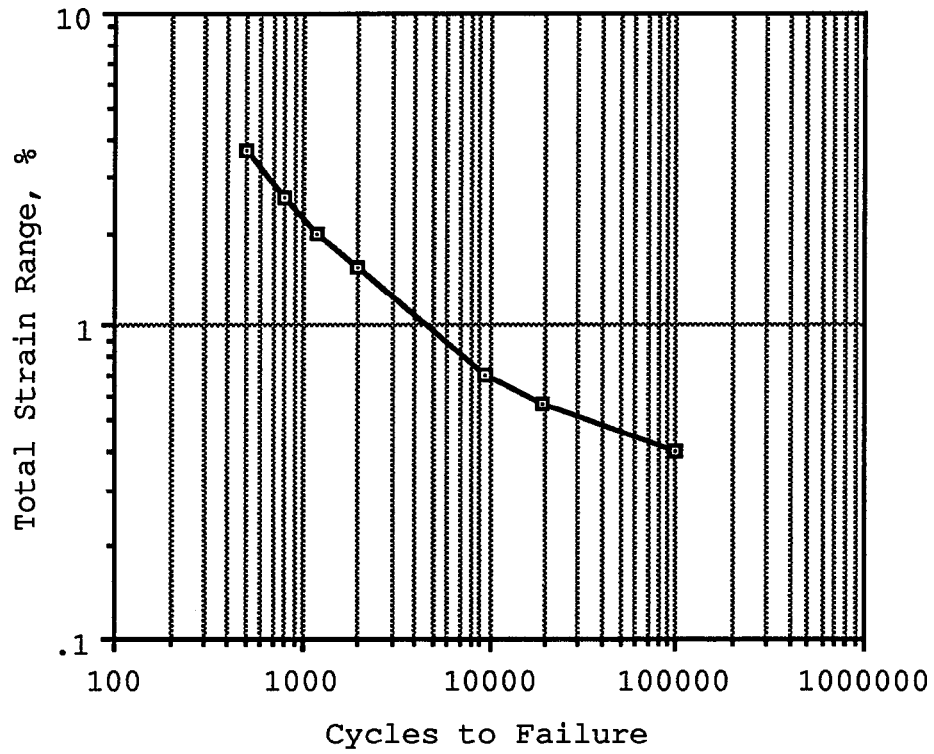


Figure 40. Total strain range vs. cycles to failure for a 2 1/4% Cr-1% Mo steel at 427 C.

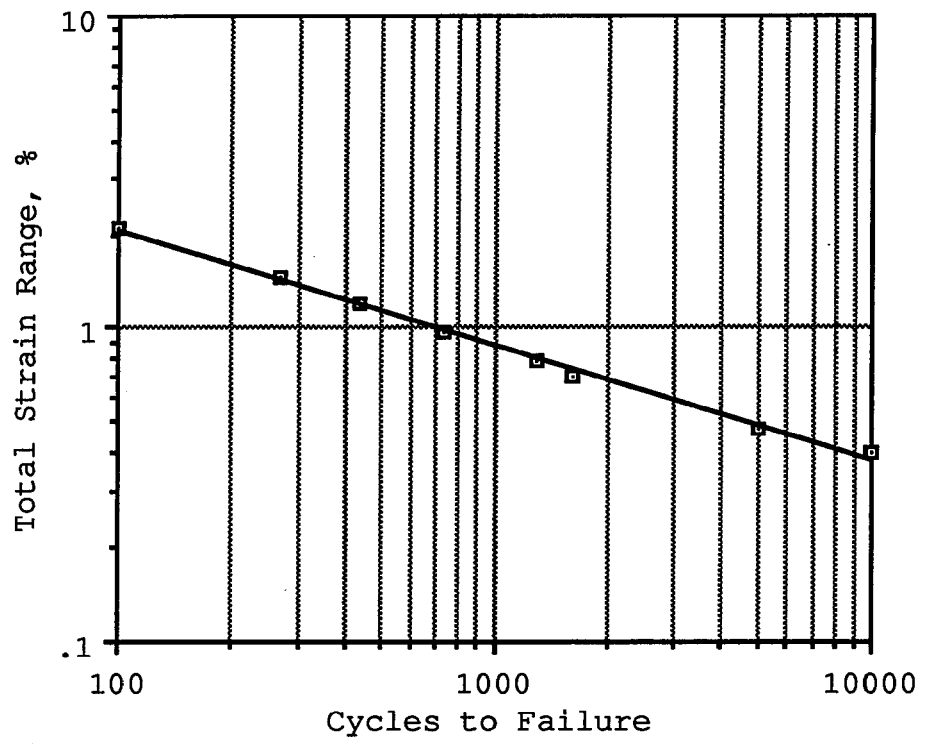


Figure 41. Total strain range vs. cycles to failure for OFHC copper at 538 C.

Table 5
Results of Analysis of Composite Tube Designs

Design	$\Delta(\epsilon_r - \epsilon_\theta)$	$\Delta(\epsilon_\theta - \epsilon_z)$	$\Delta(\epsilon_r - \epsilon_z)$	$\Delta\epsilon_{et}$	N_f	N_f	Design
3	0.02352	0.00026	0.02326	0.01559	1800		
3	0.01644	0.00004	0.01642	0.01090	450		450
24	0.00368	0.00003	0.00365	0.00244	>10 ⁵		
3	0.02031	0.00029	0.02002	0.01344	2400		
6	0.01435	0.00028	0.01423	0.00952	750		750
21	0.00390	0.00006	0.00384	0.00309	>10 ⁵		
3	0.01934	0.00031	0.01902	0.01278	2500		
9	0.01316	0.00016	0.01299	0.00872	950		950
18	0.00445	0.00005	0.00436	0.00294	>10 ⁵		
3	0.01795	0.00029	0.01765	0.01187	3500		
12	0.01169	0.00016	0.01153	0.00774	1600		1600
15	0.00512	0.00008	0.00500	0.00337	>10 ⁵		
3	0.01581	0.00019	0.01561	0.01047	3600		
15	0.00955	0.00008	0.00946	0.00633	2200		2200
12	0.00608	0.00014	0.00594	0.00401	>10 ⁵		
3	0.01331	0.00018	0.01325	0.00885	5200		
18	0.00706	0.00002	0.00708	0.00471	5200		5200
9	0.00726	0.00015	0.00712	0.00479	35000		
3	0.01064	0.00001	0.01063	0.00708	9000		9000
21	0.00392	0.00007	0.00400	0.00264	>10 ⁵		
6	0.00842	0.00000	0.00843	0.00560	21000		
3	0.00958	0.00001	0.00959	0.00639	12000		12000
24	0.00267	0.00005	0.00274	0.00180	>10 ⁵		
3	0.00769	0.00003	0.00773	0.00514	28000		
6	0.02136	0.00012	0.02125	0.01420	2100		2100
3	0.00844	0.00008	0.00852	0.00565	3200		
21	0.00362	0.00003	0.00358	0.00240	>10 ⁵		
6	0.02017	0.00011	0.02006	0.01340	2200		2200
6	0.00751	0.00006	0.00756	0.00502	3800		
18	0.00412	0.00006	0.00405	0.00270	>10 ⁵		
6	0.01909	0.00006	0.01903	0.01270	2600		2600
9	0.00618	0.00006	0.00624	0.00414	10000		
15	0.00479	0.00008	0.00471	0.00316	>10 ⁵		

Table 5 (Continued)

6	0.01746	0.00001	0.01747	0.01160	3500	3500
12	0.00451	0.00008	0.00459	0.00303	>10 ⁵	
12	0.00560	0.00008	0.00553	0.00371	>10 ⁵	
6	0.01578	0.00001	0.01579	0.01050	3800	3800
15	0.00081	0.00012	0.00094	0.00058	>10 ⁵	
9	0.00648	0.00001	0.00614	0.00421	60000	
6	0.01515	0.00004	0.01520	0.01010	3800	3800
18	0.00168	0.00004	0.00173	0.00113	>10 ⁵	
6	0.00688	0.00024	0.00691	0.00459	50000	
6	0.01517	0.00000	0.01517	0.01011	3800	3800
21	0.00041	0.00006	0.00051	0.00031	>10 ⁵	
3	0.00625	0.00002	0.00628	0.00418	>10 ⁵	
9	0.02137	0.00007	0.02124	0.01420	2100	2100
3	0.00406	0.00010	0.00417	0.00274	>10 ⁵	
18	0.00378	0.00003	0.00376	0.00250	>10 ⁵	
9	0.01995	0.00002	0.01993	0.01329	2300	2300
6	0.00378	0.00020	0.00376	0.00251	>10 ⁵	
15	0.00428	0.00003	0.00425	0.00284	>10 ⁵	
9	0.01893	0.00001	0.01894	0.01262	2600	2600
9	0.00174	0.00006	0.00180	0.00118	>10 ⁵	
12	0.00494	0.00001	0.00495	0.00329	>10 ⁵	
9	0.01919	0.00002	0.01916	0.01278	2600	2600
12	0.00160	0.00014	0.00152	0.00104	>10 ⁵	
9	0.00521	0.00002	0.00522	0.00347	>10 ⁵	
9	0.01917	0.00023	0.01914	0.01277	2600	2600
15	0.00083	0.00009	0.00085	0.00056	>10 ⁵	
6	0.00533	0.00001	0.00535	0.00356	>10 ⁵	
9	0.01906	0.00003	0.01903	0.01269	2600	2600
18	0.00065	0.00008	0.00068	0.00144	>10 ⁵	
3	0.00487	0.00000	0.00487	0.00324	>10 ⁵	
All Steel	0.02167	0.00008	0.02161	0.01443	2000	2000
All Copper	0.00813	0.00015	0.00798	0.00537	3400	3400

which represent the ID, middle, and OD layer thicknesses, respectively (listed vertically, in groups of three). These data are presented graphically in Figures 42-45. Figure 42 shows the thermal fatigue life of multilayered tube designs for three different ID layer thicknesses as a function of the copper layer thickness. The thermal fatigue life data points at 0 mm and 30 mm on the "copper layer thickness axis" of this graph are the thermal fatigue lives of an all steel and an all copper tube design of the same total thickness as the multilayered designs. The all steel and all copper designs were run on the model and are presented for comparison with multilayered designs. The OD layer thickness is not shown explicitly on this graph because it was not the life controlling constraint. Figures 43, 44, and 45 graphically illustrate the thermal fatigue life of each layer for ID layer thicknesses of 3, 6, and 9 mm, respectively. From these graphs it is apparent that the layer with the lowest thermal fatigue life determines the life of the tube.

These results indicate that the maximum thermal fatigue life of a multilayered cylindrical shell, with the system of constraints imposed on it in this demonstration analysis, occurs when the ID and OD steel layers are relatively thin and the central layer of copper is relatively thick. An optimal life of 12,000 thermal cycles was achieved for the "demonstration design" by selecting a 3 mm ID, 24 mm middle, and 3 mm OD layer thicknesses. This design had a life of

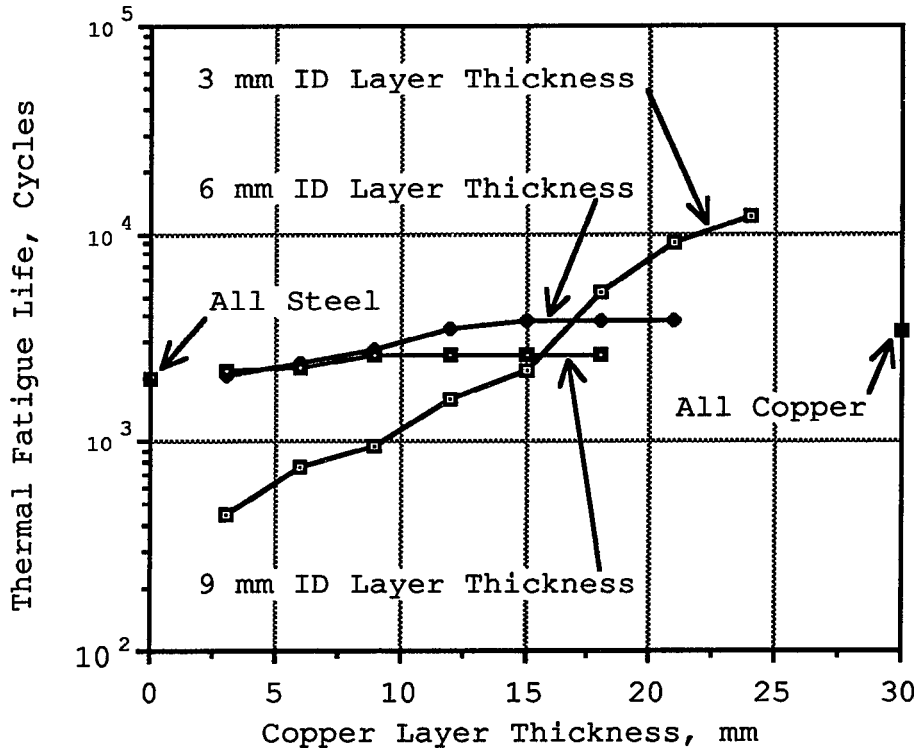


Figure 42. Thermal fatigue life of multilayered tube designs.

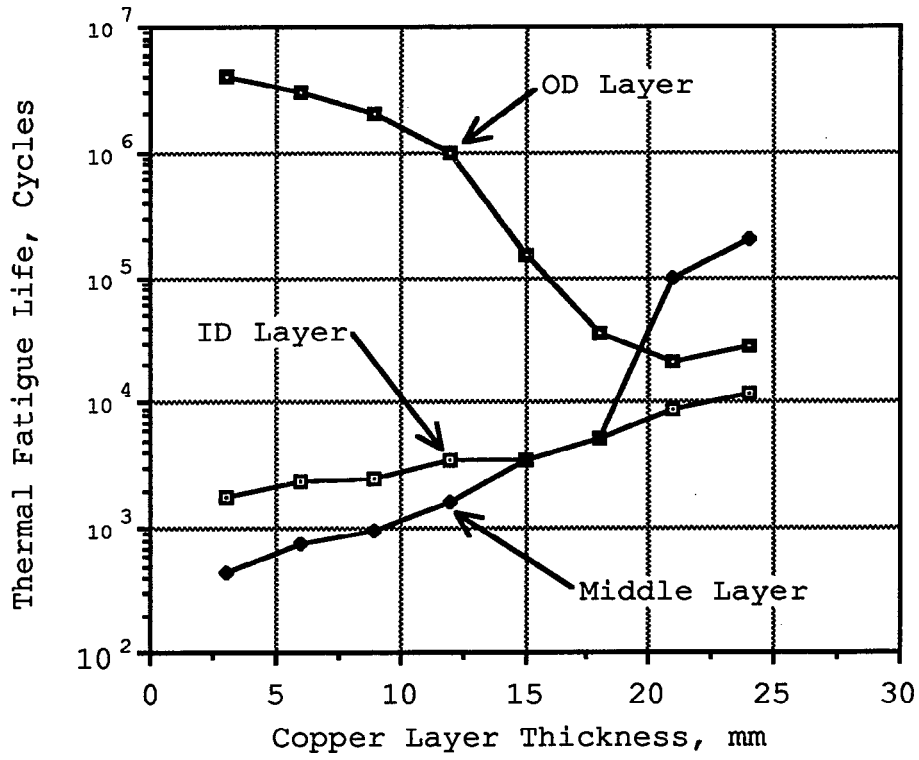


Figure 43. Thermal fatigue life of layers in multilayered tube designs with a 3 mm ID layer thickness.

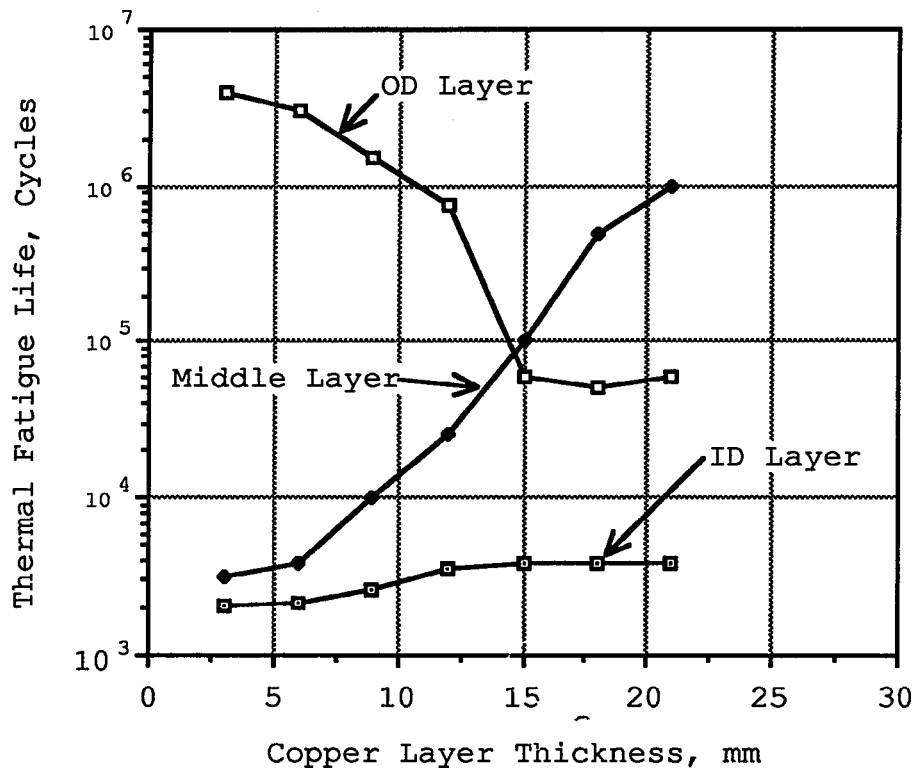


Figure 44. Thermal fatigue life of layers in multilayered tube designs with a 6 mm ID layer thickness.

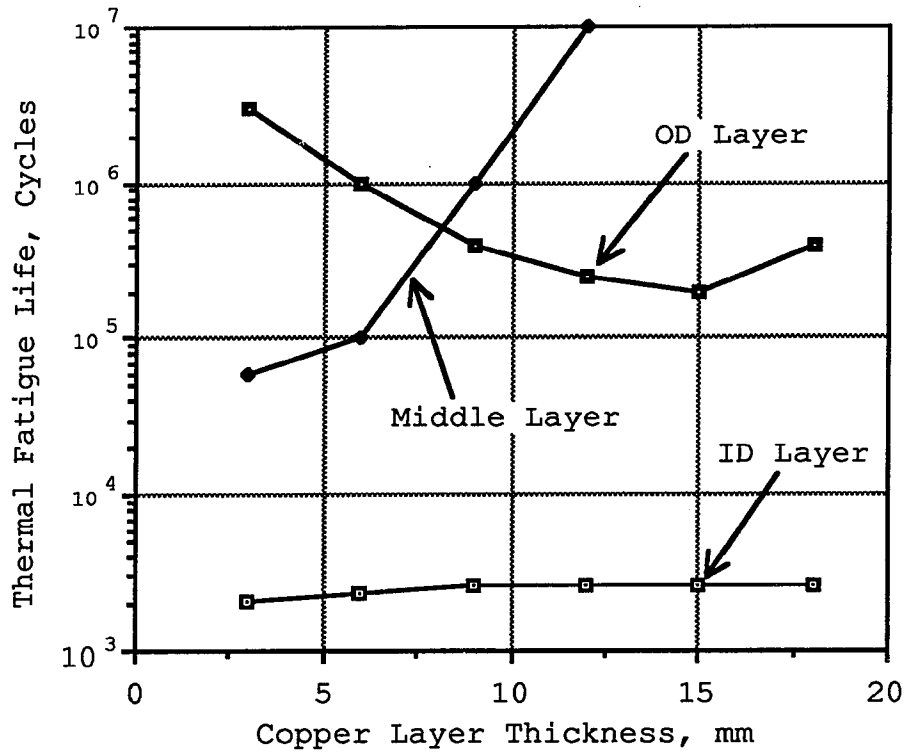


Figure 45. Thermal fatigue life of layers in multilayered tube designs with a 9 mm ID layer thickness.

about six times greater than an all steel design of the same total thickness.

It is evident from the above results that no case was presented in which the thermal fatigue life of the tube was determined by failure of the OD layer. This situation occurred because the ID steel and copper layers incurred higher strain ranges and shorter lives due to their higher mean temperature than did the water cooled OD layer.

V. DISCUSSION OF RESULTS

The results from the numerical model were analyzed to determine how well they conform to the criteria that must be satisfied for the model to have credibility. The conditions that must be satisfied were:

- (a) Radial stresses at the ID and OD surfaces must be equal to zero.
- (b) Radial stresses must be continuous.
- (c) The displacement function, $U(r)$, must be continuous and differentiable.
- (d) The tangential strain, ϵ_{θ} , must be continuous.
- (e) The axial strain, ϵ_z , must be constant.
- (f) The tube must be in equilibrium as described by equation 46 and Figure 9.

The radial stresses at 1, 10, and 35 seconds were calculated by the model as shown in Figures 19, 25, and 31. These graphs show a continuous radial stress profile with σ_r equal to zero at the ID and OD boundary surfaces as required by conditions (a) and (b). Condition (c) was satisfied as shown in Figure 46, and it followed that ϵ_{θ} , defined as U divided by r , was also continuous, which satisfied condition (d). Condition (e), a requirement for plane strain, was met as shown in Figure 47. Condition (f) was met with some qualification. Recall that during the derivation of the

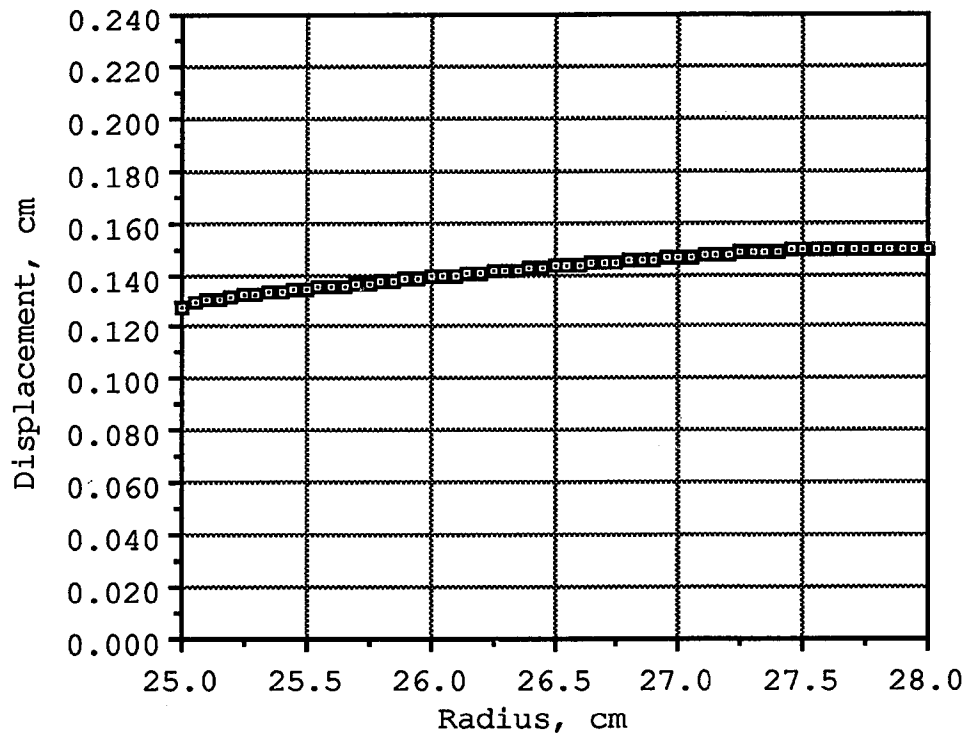


Figure 46. The radial displacement as calculated by the model, 10 seconds into a thermal cycle.

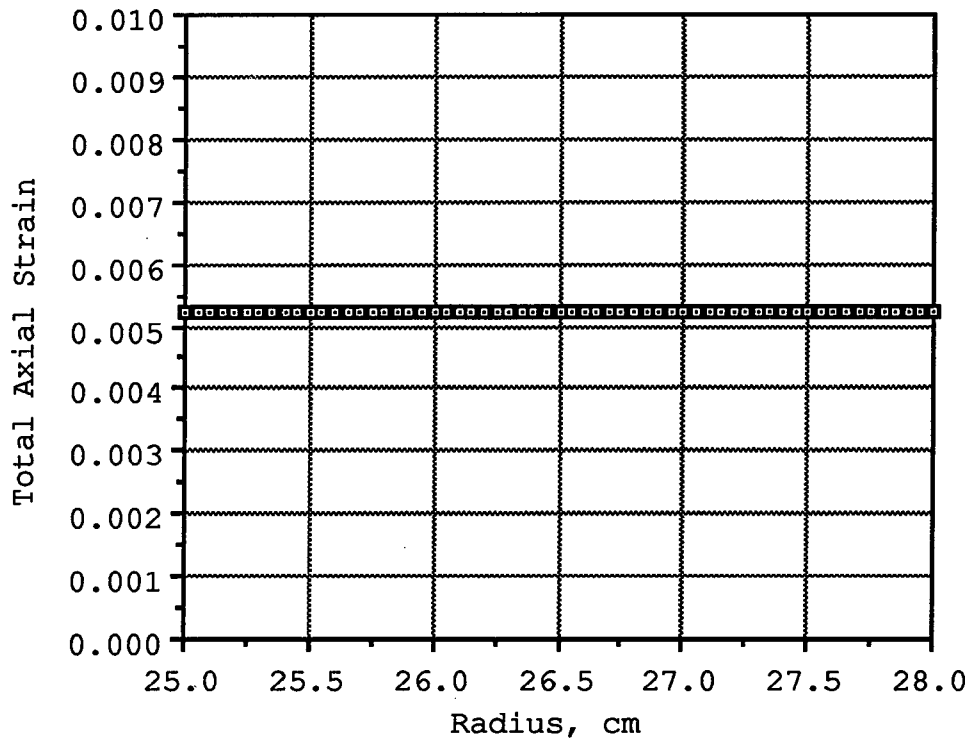


Figure 47. Plot of total axial strain, ϵ_z , across the wall thickness of the tube demonstrating that a plane strain condition exists.

strain equations, the modulus of elasticity and the thermal expansion coefficient were assumed constant because of the complexity introduced if they entered the solution as functions of radius. An approximate method was developed to treat E and α as functions of radius even though they did not enter the differential equation representing equilibrium as such. To evaluate the correctness of the analysis resulting from this technique, the form of the solution for the displacement, U , for three different types of analysis was considered. The three types of analysis were (1) elastic, (2), an elastic-plastic analysis where E and α are constant, and (3) an elastic-plastic analysis where E and α were functions of the radius. For an elastic analysis U was represented by:

$$U = \frac{1 + \mu}{1 - \mu} \frac{1}{r} \int_a^r \alpha T r dr + C_1 r + \frac{C_2}{r} \quad [112]$$

where the integral represents displacements resulting from thermally induced elastic stresses. In the second type of analysis, in which both the elastic and plastic natures of a material were taken into account, U was represented by:

$$U = \frac{1 + \mu}{1 - \mu} \frac{1}{r} \int_a^r \alpha T r dr + \frac{1 - 2\mu}{2(1 - \mu)} \frac{1}{r} \int_a^r (\epsilon_{rp} + \epsilon_{\theta p}) r dr + \frac{1 - 2\mu}{2(1 - \mu)} \frac{1}{r} \int_a^r \frac{(\epsilon_{rp} - \epsilon_{\theta p})}{r} dr + C_1 r + \frac{C_2}{r} \quad [113]$$

In the third type of analysis, where elasticity, plasticity, and changes of E and α as a function of the radius were taken into account, U had the form of:

$$U = \frac{1 + \mu}{1 - \mu} \frac{1}{r} \int_a^r \alpha T r dr + \frac{1 - 2\mu}{2(1 - \mu)} \frac{1}{r} \int_a^r (\epsilon_{rp} + \epsilon_{\theta p}) r dr +$$

$$\frac{1 - 2\mu}{2(1 - \mu)} \frac{1}{r} \int_a^r \frac{(\epsilon_{rp} - \epsilon_{\theta p})}{r} dr + C_1 r + \frac{C_2}{r} +$$

(Integrals representing the changes in E
and changes in α as a function of radius) [114]

In the third type of analysis "all" values of E and α were taken as functions of the radius. It was apparent that the third type of analysis would prove more accurate than the second type, and the second type, more accurate than the first.

In this dissertation, a modification of the third type of analysis was used, in that E and α were used as functions of radius but integrals representing the change of E and α as function of r were not included. This implies that the accuracy of the modified analysis is much greater than that of method 1 and much better than method 2 but not as accurate as method 3.

Upon calculating a numerical value for condition (f) the sum of the tangential forces across the wall was found to vary from +3.51 to -3.51 Newtons depending on which part of the thermal cycle was considered. Similar values calculated for a monolithic tube varied from +0.87 to -0.87 Newtons. Though these values were not zero, they were less than 8% of the peak forces that occurred in the tube and were felt to be within acceptable limits for optimization of one tube design with respect to another. The error is a result of not completely accounting for changes of E and α as a function of radius.

VI. CONCLUSIONS AND RECOMMENDATIONS

The goal of this dissertation was to develop a technique to determine and optimize the thermal fatigue life of a multilayered cylindrical shell. This goal was achieved through the implementation of a numerical model of sufficient flexibility to deal with the major variables affecting thermal fatigue life in a thermally cycled multilayered tube. The technique was demonstrated by optimizing the thermal fatigue life of a three layered composite tube for a specific set of constraints.

Several important conclusions were drawn as a result of this work:

1. The solutions presented for the total strain equations, ϵ_r , ϵ_θ , ϵ_z , and constants of integration C_1 and C_2 , for a cylindrical tube in terms of temperature and plastic strain were derived in this dissertation and represent a significant contribution to the literature.
2. An approximation technique to account for different E , α , and plastic flow characteristics as a function of temperature for the materials used in a multilayered composite tube design is presented in this dissertation and represents a significant contribution to the literature.

3. The combination of the heat flow and strain equations, developed in this dissertation, into a thermo-elastic-plastic numerical model of a multilayered cylindrical tube using an incremental plasticity technique is a significant contribution to the literature.
4. Using the computer model, it was found that with proper selection of layer thicknesses, the thermal fatigue life of a three layered composite design could be improved substantially compared to an all steel or all copper design of the same thickness.
5. The maximum thermal fatigue life of the designs investigated resulted when the ID and OD layers were at their minimum constrained thicknesses.
6. The strain range of the ID steel layer was always greater than the OD steel layer if the same alloys and thicknesses were used for both layers. This situation led to failure of the ID layer before failure of the OD layer could occur.

The technique developed in this dissertation was used to determine and optimize the thermal fatigue life of a tube with certain constraints. The technique is flexible and may be used for the analysis and optimization of other axisymmetric, thermally loaded multilayered tubes.

The technique may be expanded to include additional layers or may be reduced to analyze single or double layered shells. The technique is highly recommended because of the insight it gives a designer with respect to the major

variables affecting the thermal fatigue life of ID or OD heated tubing. The effects of heat transfer coefficients, heat source temperatures, cycle times, and cooling water temperatures may be varied to determine the effect on the thermal fatigue life of a design. From plastic strain calculations and with experimental verification the model could also be used to determine the geometric stability of a design under certain thermal loading conditions.

LIST OF REFERENCES

- 1 J.M.C. Duhamel: "Memoires...par Divers Savants," vol. 5 p. 440 Paris, France 1838.
- 2 S.P. Timoshenko and J.N. Goodier: Theory of Elasticity. 3rd ed., McGraw-Hill Book Company. 1970, pp. 441-449.
- 3 A. Mendelson and S.S. Manson: Practical Solution of Plastic Deformation Problems in the Elastic-Plastic Range. American Society of Mechanical Engineers Paper No. 56-A-202. October, 1956.
- 4 R.S. Hanson: Ph.D. Dissertation, Iowa State College, 1958.
- 5 S.S. Manson: Thermal Stress and Low-Cycle Fatigue, Robert E. Krieger Publishing Company, Malabar, FL. 1981, pp. 224-240.
- 6 L.F. Coffin, Jr.: A Study of the Effects of Cyclic Thermal Stresses on a Ductile Metal, Trans. ASME, vol. 76, p. 923, 1954.
- 7 G.E. Myers: Analytical Methods in Conduction Heat Transfer. McGraw-Hill. 1971, pp. 293-297.
- 8 S.H. Crandall and N.C. Dahl, eds: An Introduction to the Mechanics of Solids. 2nd ed., McGraw-Hill Book Company. 1972, pp. 337-346.
- 9 S.S. Manson: Thermal Stress and Low-Cycle Fatigue, Robert E. Krieger Publishing Company, Malabar, FL. 1981, p. 91.
- 10 S.S. Manson: Thermal Stress and Low-Cycle Fatigue, Robert E. Krieger Publishing Company, Malabar, FL. 1981, p. 92.
- 11 S.S. Manson: Thermal Stress and Low-Cycle Fatigue, Robert E. Krieger Publishing Company, Malabar, FL. 1981, p. 92.
- 12 W.M. Rohsenow, J.P. Hartnett, and E.N. Ganic, eds. Handbook of Heat Transfer Fundamentals. 2nd ed. McGraw-Hill Book Company. 1985, pp. 5-20.

LIST OF REFERENCES (Continued)

- 13 M.R. Hill, compiler: Mechanical Properties Test Data for Structural Materials Quarterly Progress Report for Period Ending July 31, 1974. Oak Ridge National Laboratory. Contract No. W-7405-eng-26.
- 14 J.B. Conway, R.H. Stentz, and J.T. Berling: High Temperature, Low-Cycle Fatigue of Copper-Base Alloys in Argon; Part I - Preliminary Results for 12 Alloys at 1000 °F (538 °C), National Aeronautics and Space Administration, Report No. NASA CR-121259. Jan. 1973, p. 30.

GRADUATE SCHOOL
UNIVERSITY OF ALABAMA AT BIRMINGHAM
DISSERTATION APPROVAL FORM

Name of Candidate Gene L. Oliver

Major Subject Materials Engineering

Title of Dissertation AN ANALYTICAL METHOD TO OPTIMIZE THE
THERMAL FATIGUE LIFE OF MULTILAYERED CYLINDRICAL SHELLS

Dissertation Committee:

J. Barry Andrews, Chairman Burton R. Patterson
Rose Adams
Ray Thompson
A. Eugene Carden

Director of Graduate Program J. Barry Andrews

Dean, UAB Graduate School Anthony Ramo

Date 9/2/88